BROAD-BAND COLORS OF VIRGO CLUSTER LSB DWARF IRREGULAR GALAXIES

Ana B. Heller and Noah Brosch

The Wise Observatory and the School of Physics and Astronomy

Tel Aviv University, Tel Aviv 69978, Israel

Received _____; accepted _____

ABSTRACT

We present UBVRI images and surface photometry of a complete sample of 29 low-luminosity dwarf irregulars galaxies in the Virgo Cluster, for which we derive central surface brightnesses, scale lengths, integrated magnitudes, and median colors. The color distributions are discussed in terms of radial surface brightness profiles, and color gradients are interpreted and compared with corresponding ones for low surface brightness spiral galaxies. By combining broad-band and narrow-band filter observations, the past and current role of the cluster environment on the evolution of LSB dwarf irregular galaxies is evaluated.

Keywords: LSB dwarf irregular galaxies, Virgo cluster, surface photometry.

1. Introduction

Faint galaxies with B-band central surface brightnesses $\mu_0 > 23.0$B mag arcsec^{-2} are known as low surface brightness galaxies (LSBs). Their evolution, both in the field as well as in cluster environments, remains uncertain.

In the field, the best-studied cases of LSBs are blue spirals (for a summary of their properties and references see de Blok 1997). These objects show few traces of star formation and are inferred to be rather young, but slowly evolving systems. This is because their colors ($U-B < -0.2$, $B-V < 0.6$, $V-I < 1.0$) are often similar to those of star-forming late-type spiral galaxies (Sd/Sc), and their metallicity is low ($Z \leq 0.3 Z_{\odot}$) (McGaugh & Bothun 1994). Generally, they have high M_{HI}/L fractions and their average HI surface density is lower than the critical threshold for star formation (SF) onset. Their rotation curves indicate that they are dark-matter dominated and are therefore probably stable to external star formation triggers that may accelerate SF processes (Mihos *et al.* 1997).

A proposed explanation for the color of LSB galaxies is that the formation of massive stars is generally suppressed in these objects due to the low initial gas density. In a cluster environment, unlike their young blue counterparts in the field, these galaxies may have had increased star formation rates (SFRs) in the past, due to distant tidal interactions with other galaxies, and today these LSBs may be fading (Tailor 1997). It is then reasonable to assume that if the evolution of LSB galaxies was accelerated in cluster environments, then cluster environments may contain more red LSBs than the field. Significant numbers of very red ($U-B \geq 0.3$, $B-V \geq 0.8$) LSB spirals galaxies in the Cancer and Pegasus clusters have already been found, in support of this possibility (O'Neil *et al.* 1997a,b, 2000).

As the size of the system is reduced, the stochastic self-propagating star formation

model (SSPSF, Gerola & Seiden, 1980) predicts a higher probability for a galaxy to experience large fluctuations that could temporarily halt the star formation than in a sparse environment. Consequently, if the cluster environment accelerates the evolution of intrinsically small galaxies, as O'Neil proposes for giant LSBs, then we should expect the cluster environment to be very hostile to the survival of small, fragile-looking blue LSBs. However, color surveys of dwarf galaxies in the Fornax and the Virgo clusters do not show evidence for an abnormal number of red LSB galaxies. Most of the galaxies show colors similar to those of field galaxies: $0.0 \leq B-V \leq 0.9$ and $-0.3 \leq U-B \leq 0.3$ (Evan, Davies & Phillips 1990; Bothun *et al.* 1986 [BMCM]; Bothun *et al.* 1991; Gallagher & Hunter 1986 [G&H], Gallagher & Hunter 1989). G&H raise the possibility that the bluest Im/Sm galaxies could be, in fact, high surface-brightness galaxies (HSBs). For excellent reviews of the star formation and other properties of dwarf irregular galaxies as a class, see for example Gallagher (1996), Hunter (1997), or van Zee (2000) and references therein.

In order to constrain the LSB dwarf population of the Virgo cluster, and thus to attempt an evaluation of the role of their environment on their evolution, we present in this paper UBVRI surface photometry of a complete sample of low luminosity Magellanic irregular galaxies in the cluster. The Hα continuum and line images of the sample were analyzed in Heller *et al.* (1998, 1999) where the entire sample was described. The luminosity density and the size of the galaxies in the UBVR and I passbands are approximated here by radial luminosity profiles. Usually, the light distribution in galaxies is assumed to be either exponential $\Sigma(r) = \Sigma_\circ e^{-r/h}$ (for disks) or $r^{-1/4}$ (for spheroidal). In this study we consider also a generalized exponential distribution of the form $\Sigma(r) = \Sigma_\circ e^{(-r/h)^n}$, where n is a free parameter characterizing the gradient of the light intensity as a function of radius. This kind of luminosity profile was first described by Sersic () and we call it here a 'Sersic profile' (Sersic, 1968). Note that any luminosity profile analysis assumes that the flux is azimuthally symmetric across the object; this is

very often not the case in dwarf irregular galaxies (Brosch *et al.* 1998; Heller *et al.* 2000).

The paper is organized as follows: first, we present the UBVRI images, we derive the cumulative brightness, the surface brightness and color profiles, the typical color indices, and the surface photometry parameters for each galaxy. We also perform a statistical analysis of the goodness of fit for four kinds of intensity profiles. We then discuss the results and compare them to those of LSB spiral galaxies. Finally, we evaluate the role of the cluster environment on the star formation process in LSB dwarf irregular galaxies (DIGs).

2. Observations and surface photometry

Our sample consists of 29 low-luminosity Magellanic irregular (Im) galaxies in the Virgo cluster selected from the VCC catalog (Binggeli, Sandage, & Tammann, 1985) that are classified ImIV or ImV. The selection is based on single-dish non-zero HI measurements from Hofffman *et al.* (1987, 1989a,b) and the sample is complete to $m_B \leq 17.2$. Galaxy VCC 2037, although included in the sample, was not analyzed here because of a superposed bright star on all images. Membership is assured by the HI heliocentric velocity $v_\odot < 3000$ km sec^{-1}, which is within the redshift range of the Virgo cluster. The typical optical diameter of a galaxy in the sample is one arcmin. Assuming a uniform sample distance of 18 Mpc ($h = H_\circ/75$), with a plate scale $1'' = 87.3$ pc, this size correspond to 5.2 Kpc. The galaxies were imaged through broad-band U, B, V, R, I, and narrow-band Hα (in the rest frame of each galaxy) filters with the Tel Aviv University's 1.0-m telescope at the Wise Observatory (WO). The instruments used were a CCD camera mounted at the $f/7$ of the telescope, using either a 1024×1024 pixel^2 Tektronics (TEK) CCD or a 512×512 pixel^2 RCA CCD as its detector. The resolution in these configurations is 0.7"/pixel or 0.9"/pixel respectively with a typical seeing size of ≈ 2.5 arcsec. A few objects were imaged with a Faint-Object-Spectrograph-and-Camera

(FOSC)/TEK configuration, with a plate scale of 2.08"/pixel. For each galaxy we obtained total exposures from 2700 up to 5400 seconds (broken into three exposures per band), according to the filter transmission.

Co-added images were derived using standard data reduction techniques from IRAF; these include flat-fielding, removing of cosmic rays, spatial registration, convolution to the point-spread function of the image with the poorest resolution, and median-combining of the matched images. The background was then subtracted from the output image as a tilted surface, which was derived by fitting a second order polynomial to the combined image, with the galaxy and all other bright objects masked-off. The measurements were put on an absolute scale by observations of Landolt (1973, 1983) standard stars in equatorial regions over a range of air-masses, and calibrating as secondary standards up to five stars in the field of each galaxy.

Standard photometric methods, using circular or elliptical apertures, cannot describe well the light intensity of irregular galaxies. These irregular shapes generally require the use of large apertures for which too much sky noise is included; the best choice to perform integrated photometry should be with a confinig polygon traced around the galaxy. This method was used by Almoznino & Brosch (1998, A&B) and was also applied to the Hα and red continuum analysis in Heller *et al.* (1999). The disadvantages of the polygonal aperture method are that it does not allow a surface photometry analysis, and that the integrated photometry results are difficult to compare with those published by other authors. In this paper we adopt the method of ellipse-fitting multi-aperture photometry with fixed position angle and ellipticities, at one pixel intervals. The outermost isophote to which we integrate is defined as the location where the total magnitude, 'curve of growth' levels off in each band. The ellipse parameters are from Heller *et al.* (2000). Errors in intensity, magnitude and local gradients include the rms scatter of the intensity data along the fitted ellipse, the rms error in the sky subtraction, and errors from the

absolute photometry of the calibration stars. These were added in quadrature to obtain the final measurement errors.

We use four different models fitted to the B-band surface brightness profiles: *(a)* an exponential profile, with a free index n given by $\mu = \mu_\circ + 1.086 \times (r/h)^n$, where $\mu_\circ$ is the extrapolated central surface brightness in mag arcsec^{-2} and h is the scale length in arcsec (the Sersic profile), *(b)* a pure exponential disk with $n = 1$ [special case of *(a)*], *(c)* a spheroidal distribution given by $\mu = \mu_e + 8.33 \times [(r/r_e)^{1/4} - 1]$, where μ_e is the effective surface brightness in mag arcsec^{-2} and r_e is the half-light radius in arcsec, and *(d)* a combined central spheroid (bulge) and outer disk components given by $\mu = \mu_c + 1.086 \times (r/h) + 8.33 \times (r/r_e)^{1/4}$, where μ_c is the central bulge+disk surface brightness. Typical examples of the four models are plotted in Fig. 1. The fitting starts normally at a galactocentric distance of 3.5-4.5 arcsec, and extend to locations with a surface brightness level of μ_B=27 mag arcsec^{-2}. We estimate the quality of the fit with reduced χ^2 statistics (χ^2/df), averaging every two data points. This approach reduces the quality of the fit by a factor of approximately two, but accounts for possible influences of the seeing.

Color profiles U-B, B-V, V-R, and R-I are derived by subtracting two individually-determined surface brightness profiles at one-pixel intervals, and the errors are estimated by adding the two measurement errors in quadrature. The average and median colors of the galaxy are calculated from all derived color values, from the minimal to the maximal apertures. We adopt this method to obtain the representative underlying color of the continuum in LSB galaxies because it avoids over-weighting the brighter parts of a galaxy. Color gradients are estimated by a linear least-square fit to the color profiles.

3. Results and discussion

The major limitations when analysing surface photometry of DIGs are the uncertain absorption and inclination corrections. The surface brightness in mag arcsec^{-2}, corrected for inclination (I), internal dust extinction (A_{int}), and extinction in the Galaxy (A_{gal}), is: $\mu_{corr} = \mu - A_{gal} - A_{int} - A_I$ where $A_I = 2.5 \times log[cos(I)]$, and $cos(I) = b/a$ is derived from ellipse fitting and is corrected for the intrinsic axial ratio $q_\circ$ (often taken to be 0.2), by $cos^2(I) = \frac{(b/a)^2 - q_\circ^2}{1 - q_\circ^2}$.

Since the galactic extinction in the direction of Virgo is negligible, it is reasonable to take $A_{gal} \approx 0$. Inclination corrections A_I carry on the uncertainty in the axis ratio (b/a). For the internal dust extinction corrections A_{int} one assumes an empirical extinction law; for example, A&B evaluated typical color excesses E(B-V)=0.17, E(V-R)=0.1, E(R-I)=0.13, and E(UV-V)=0.92 for BCD galaxies in the Virgo cluster. This was based on the median difference in optical depths, $\tau \approx 0.4$ of the Hβ and Hα lines derived by Calzetti *et al.* (1994) for a sample of star-burst galaxies. However, in view of the uncertainty of these values, mostly due to effects of metallicity and age of the stellar population on the B band, we list here observed parameters uncorrected for these effects.

In Fig. 2 through Fig. 30 we show for each galaxy the images in the U, B, V, R, and I pass-bands in the *left* panel of each figure. The *lower-right* panel shows color profiles derived from the surface brightness distribution, the *top-middle* panel shows surface brightness profiles in all broad bands, and the *top-right* panel displays cumulative magnitude profiles as a function of increasing aperture in arcsecs. The light distributions of the surface brightness profiles are generally smooth, as expected from a mix of stellar populations. Stronger irregularities are present in the U-band profiles, reflecting the sensitivity of this passband to the younger population formed in the last starburst. As this is the passband with the lowest signal-to-noise, the errors bars are plotted there for each point and they represent upper limits for error bars in all bands. Note that the

galaxy VCC 169 is not included in the statistical results due to the low S/N in all the images. A second galaxy we did not include is VCC 2034; for this object we only show the images in all pass-bands but a superposed bright star, covering most of the galaxy, does not allow us to perform accurate surface photometry.

To derive the level of significance of the fitting of the different models we use reduced χ^2 statistics. The fitting indicates that the appropriate law of brightness distribution is nearly Gaussian, with a median exponent index $n = 1.74 \pm 0.86$. The scale lengths in the B-band for the sample galaxies cover the range $7 \leq h_B \leq 38$ arcsec, that is, the range of 0.6-3.3 Kpc; this is approximately half the R_{27} isophote (Table 1). For 15% of the galaxies a pure ($n = 1$) disk model would also make a suitable choice (Table 2). A disk+bulge model fits 15% of the galaxies to a $\chi^2 \leq 1.6$ (5% significance), and *none of the galaxies can be fitted with a* $r^{1/4}$ *law.* Note that, in all cases, the fitted radii of the bulges (r_e) are too close to the seeing size of the images to be considered reliable (Table 3). The central surface brightness values, derived from the exponential profile fits, confirm that the objects are LSB galaxies, with $\mu_\circ \geq 23.0$ mag arcsec^{-2} in the B-band. The only analysed galaxy with a brighter central surface brightness is VCC 83; this is classified Im III-IV in VCC.

In Table 4 we list mean and median color indices, the standard deviation (σ), and the number (N) of data points from which these values were derived. For those cases where the distribution is not symmetrical, the mean and the median are not longer equal. The mean is mostly affected by strongly deviant pixels, thus it is the median that provides the best estimate of the typical color. For comparison, we repeat in Table 6 color indices reported by BCML, G&H, and A&B for the objects in common with our sample. BCML give color indices at two apertures: one of 11 arcsec for all the galaxies, and a second larger and elliptical. G&H provide information for only one circular aperture, and A&B give this for one polygon. The typical average uncertainty of those studies is 0.03 -

0.08 mag, which is comparable with the uncertainty of our annular aperture photometry for most of our galaxies. The differences of listed magnitudes and errors in Tables 4 vs. Table 6 are a consequence of the different methods of measurement; BCML, G&H, and A&B derive integrated color indices, thus most of the weight is given to the luminous parts of a galaxy, while we assign here the same statistical weight to all data points of the profiles. Only for a constant surface brightness both methods should give the same results in magnitude and errors. Note also that we neglected color terms smaller than 0.03 mag. However, a comparison of previously published results to ours shows generally good agreement (within one standard deviation).

It is possible to divide the galaxies into three categories: the very blue, the very red, and the combined case. The galaxies in the very blue category are those with $U-B<-0.2$, $B-V<0.6$, $V-I<1.0$; they represent 30% of the sample. The galaxies in the very red category have $U-B>0.3$, $B-V>0.8$, $V-I>1.0$. None of the galaxies in the sample fall in this category. Most of the galaxies, 70%, are in the third group, with intermediate colors: $-0.4<U-B<0.6$, $0.1<B-V<0.8$, and $0.30<V-I<1.2$. These galaxies can be interpreted as combinations of different stellar populations, represented by the <200 Myr stars, ≈ 1 Gyr stars, and a population >5 Gyr belonging to previous stellar generations. The older populations seems not to be strong; in general, the galaxies tend to contain a mix of young and middle-age populations. We conclude, therefore, that the absence of very red galaxies indicates that the evolution of LSB dwarf galaxies is not accelerated by the cluster environment.

An alternative method to track star formation histories in late-type dwarf galaxies is based on color gradients. While color gradients may be degenerate in age and metallicity, it is reasonable to assume that DIGs, due to their low metallicity content, do not have strong metallicity gradients. Thus, strong color gradients should imply differences in the mean age between the inner and outer parts of a galaxy. This effect should be more

sensitive to the recent young population in the (U-B) color. Age gradients are common in late spiral galaxies (de Block 1997; Bell *et al.* 2000); the detected color gradients per B-band scale length are $-0.07 < \delta(U-B) < -1.20$, $-0.02 < \delta(B-I) < -0.60$. These negative gradients are consistent with typically younger outer regions. In isolated DIGs color gradients are reported to be generally very small or negligible. However, many compact galaxies are dramatically redder in their outer region (Patterson & Thuan 1996; van Zee 2000). To somehow quantify these gradients, and lacking numerical information, we applied linear eye fits to the published color profile plots of Patterson & Thuan and of van Zee, and found $\delta(U-B) < \pm 0.5$, $\delta(B-I) < \pm 0.4$. This can be compared with the color gradients along the full extent of the galaxies in our cluster sample. These are derived by applying an error-weighted linear fit to the color profiles, while averaging every two data points. The results and significance of these fits are listed in Table 5, where Δ_{color} represents the color gradient per arcsec. We include, for reference, the scale lenght h_B from the exponential model with free index n (Sersic profile) from Table 1. Diagrams of color-color gradients per h_B are ploted in Fig. 31. Some galaxies show very small gradients, as normally expected in irregular galaxies. However, there are also objects with strong negative or positive gradients. Note that the statistical significance (in χ^2 terms) of a linear distribution is generally poor, which implies a distribution that is not smooth with the radius. We believe that these properties are naturally explained by the number and the distribution of the regions where stars formed in different generations, inherent in the lopsideness ($A_{H\alpha}$) of DIGs analysed in detail by Heller *et al.* (2000). This effect is illustrated in Fig. 32, where we plot $\delta(B-I)$ versus $A_{H\alpha}$ for all the sample galaxies with detected Hα emission. The plot shows that the more asymmetric the Hα emission is, the larger the color gradients can become. This also explains why the gradients can reach large values in DIGs, and also why the gradients can be negative or positive, contrary to the systematic negatives gradients found in spiral galaxies.

4. Summary

We conclude that the classification ImIV-V from the VCC catalog, implying low surface brightness, that is, central surface brightness fainter that 23 mag arcsec^{-2} has been confirmed. The radial light distribution of these galaxies is described well by a Sersic model with exponential profiles of index $1 \leq n \leq 2$. LSB galaxies can be as blue as HSB galaxies. We confirm the expectation that there is no dependence between color and surface brightness. The stellar population is probably a mixture of middle-age and young stars combined with traces of an old population. None of these galaxies can be considered very red and it seems that the cluster environment did not accelerate their past star formation process. The cluster is also not affecting the current star formation process, as our measurements with narrow-band Hα filters indicate a only modest star formation rate. Finally, the lack of systematic negative color gradients in our sample galaxies is a very interesting result, because it implies that the physical mechanisms by which negative gradients are generated in LSB spiral galaxies are not dominant in LSB dwarfs. A random mechanism of star formation, whereby stars form at any given location within a galaxy, can explain the properties observed in LSB dwarfs irregular galaxies (Heller *et al.* 2000).

This study was supported by a Center of Excellence grant from the Israel Science Foundation and by the Austrian Friends of Tel Aviv University. AH is grateful to the Sackler Institute of Astronomy at Tel Aviv University for a grant to allow participation at scientific meetings. An anonymous referee contributed constructive remarks that improved this paper.

REFERENCES

Almoznino E., Brosch N., 1998, MNRAS, 298, 920, (A&B)

Bell E. F., Barnaby D., Bower R. G., de Jong R. S., Harper D. A., Hereld M., Loewenstein R. F., Rauscher B. J., 2000, MNRAS, 312, 470

Binggeli B., Sandage A., Tammann G.A., 1985, AJ, 90, 1681

Bothun G. D., Mould J. R., Caldwell N., MacGillivray H. T., 1986, AJ, 92, 1007, (BMCM)

Bothun G. D., Impey C. D., Malin D. F., 1991, ApJ, 376, 404

Brosch N., Heller A. B., Almoznino E., 1998, MNRAS, 300, 1091

Calzetti D., Kinney A. L., Storchi-Bergmann T., 1994, ApJ, 429, 582

de Blok W. J. G., 1997, PhD thesis, Univ. Groningen

Evans R., Davies J., Phillipps S., 1990, MNRAS, 245, 164

Gallagher J. S., Hunter D. A., 1986, AJ, 92(3), 557 (G&H)

Gallagher J. S., Hunter D. A., 1989, AJ, 98, 806

Gallagher J. S., 1996, in Leitherer C., Fritze-von-Alvensleben U., Huchra J., ed., ASP Conf. Ser. Vol. 98, From Stars To Galaxies, Astron. Soc. Pac., San Francisco, p. 315

Gerola H., Seiden P. E., Schulman L. S., 1980, ApJ, 242, 517

Heller A. B., Almoznino E., Brosch N., 1998, in Davies J. I, Impey C., Phillipps S., ed., ASP Conf. Ser. Vol. 170, The Low Surface Brightness Universe, Astron. Soc. Pac., San Francisco, p. 282

Heller A. B., Almoznino E., Brosch N., 1999, MNRAS, 304, 8

Heller A. B., Brosch N., Almoznino E., Van Zee L., Salzer J. J., 2000, MNRAS, 316, 569

Hoffman G. L., Helou G., Salpeter E. E., Glosson J., Sandage A., 1987, ApJS, 63, 247

Hoffman G. L., Williams H. L., Salpeter E. E., Sandage, A., Binggeli B., 1989a, ApJS, 71, 701

Hoffman G. L., Helou G., Salpeter E. E., Lewis B. M., 1989b, ApJ, 339, 812

Hunter D. A., 1997, PASP, 109, 937

Landolt A. U., 1973, AJ 78, 958

Landolt A. U., 1983, AJ 88, 439

McGaugh S. S., Bothun G. D., 1994, AJ, 107, 530

Mihos C., McGaugh S., de Block W.. 1997, ApJL, 477, L79

O'Neil K., Bothun G. D., Cornell M. E., 1997, AJ, 113, 1212

O'Neil K., Bothun G. D., Schombert J. M., Cornell M. E., Impey C. D., 1997 A. J, 114, 2448

O'Neil K., Bothun G. D., Schombert, J. M., 2000, AJ, 119, 136

Patterson R. J., Thuan T. X., 1996, ApJ Supplement Series, 107, 103

Sersic J. L., Atlas de galaxias australes, Observatorio Astronomico, Cordoba

Tailor C. L., 1997, ApJ 480, 524

van Zee L., 2000, AJ, 119, 2757

Table 1. Exponential model

VCC	$\mu_\circ$	h_B	n	χ^2
17	23.82 ± 0.04	25.73± 0.75	1.67± 0.08	1.61
83	22.37 ± 0.05	10.64± 0.23	1.29± 0.03	1.8
168	23.59 ± 0.33	6.26 ± 1.25	1.74 ± 0.46	0.42
169	24.94 ± 0.13	29.52 ± 3.06	2.13 ± 0.69	3.01
217	24.29 ± 0.02	38.67± 0.52	1.24± 0.05	2.24
260	23.92 ± 0.07	13.68 ± 0.69	1.71± 0.15	0.77
328	23.16 ± 0.14	14.44± 0.33	1.42± 0.04	1.61
329	23.88 ± 0.09	7.84± 0.44	1.60± 0.12	1.08
350	23.10 ± 0.26	12.88 ± 2.13	0.99± 0.15	1.65
367	23.64 ± 0.10	14.48 ± 1.65	0.90± 0.10	0.78
381	24.35 ± 0.03	25.88± 0.10	4.20± 0.21	0.42
477	24.85 ± 0.04	20.58± 0.32	2.53± 0.26	1.58
530	23.57 ± 0.09	6.43± 0.63	0.52± 0.02	2.52
565	23.96± 0.07	15.51± 0.19	3.31± 0.56	0.52
584	23.13 ± 0.23	6.10± 2.97	0.91 ± 0.19	1.47
826	23.13 ± 0.21	21.04± 0.12	1.3 ± 0.01	12.27
963	22.93± 0.06	6.49± 0.96	0.96± 0.10	2.24
1013	23.43± 0.08	9.76± 0.70	1.29± 0.11	0.81
1455	22.80 ± 0.36	8.11± 0.44	1.08± 0.05	2.32
1465	23.74± 0.02	20.91± 0.20	2.23± 0.04	0.56
1468	22.92± 0.07	23.75± 0.13	2.69± 0.11	0.11
1585	23.23± 0.11	22.49± 0.22	1.38± 0.03	1.71
1753	23.39± 0.03	10.57± 0.24	1.92± 0.08	0.42
1784	24.76± 0.02	26.11± 0.39	1.75± 0.10	1.5
1816	23.53± 0.22	18.60± 4.11	0.90± 0.14	0.57
1822	22.94± 0.13	14.82± 0.40	1.26± 0.04	1.36
1952	23.83± 0.05	16.65± 0.68	1.35 ± 0.08	1.77
1992	23.89± 0.11	23.06± 1.44	1.97± 0.17	0.43

Note. — Fitting parameters to an exponential profile with free index n. $\mu = \mu_\circ + 1.086 \times (r/h)^n$. $\mu_\circ$ is the B-central surface brightness in mag arcsec^{-2}, h_B is the B- scale length in arcsec, and n is the best fit exponent index, χ^2 is defined here as χ^2/df where df is the degree of freedom.

Table 2. Disk model

VCC	$\mu_\circ$	h_B	χ^2
17	23.44 ± 0.06	18.23± 0.23	8.32
83	22.23± 0.11	7.49 ± 0.03	3.52
168	22.89 ± 0.05	3.67± 0.14	0.79
169	24.65 ± 0.19	27.19± 8.13	3.02
217	24.16± 0.07	35.23± 0.47	2.77
260	23.42 ± 0.05	9.00 ± 0.17	3.96
328	22.72 ± 0.03	10.32± 0.039	12.57
329	23.37 ± 0.03	5.12± 0.06	3.14
350	22.91 ± 0.14	13.45 ± 0.05	1.7
367	23.71 ± 0.05	15.76 ± 0.17	0.98
381	24.11± 0.08	35.12± 0.98	17.37
477	24.42 ± 0.03	15.76± 0.33	13.25
530	23.56± 0.06	16.88± 0.04	16.42
565	23.47± 0.08	13.20 ± 1.48	1.78
584	23.28 ± 0.09	9.67 ± 0.17	1.70
826	22.73 ± 0.11	16.07± 0.06	19.23
963	22.99 ± 0.05	6.83 ± 0.08	2.00
1013	23.09± 0.03	7.23± 0.13	1.08
1455	22.39 ± 0.12	7.32± 0.10	2.45
1465	23.46 ± 0.03	19.59± 0.15	8.05
1468	22.47± 0.05	18.07± 0.15	27.51
1585	23.00± 0.03	17.74± 0.27	5.17
1753	22.86± 0.12	6.83 ± 0.13	19.61
1784	24.48 ± 0.02	20.63± 0.12	9.4
1816	23.59± 0.02	19.86± 0.40	0.55
1822	22.74± 0.02	12.23± 0.01	4.85
1952	23.58 0.01±	13.24± 0.10	6.23
1992	23.09 0.05±	12.41± 0.23	2.98

Note. — Reduced χ^2 statistics and fitting parameters to a disk profile $\mu = \mu_\circ + 1.086 \times (r/h)$. $\mu_\circ$ is the B- central surface brightness in mag arcsec^{-2}, h_B is the B-scale length in arcsec.

Table 3. Bulge+disk model

VCC	μ_c	h_B	r_e	χ^2
17	23.44 ± 0.02	18.24± 0.24	5.36 ± 4.70	8.74
83	22.03 ± 0.05	7.50± 0.03	1.60± 1.94	3.83
168	22.89 ± 0.05	3.67 ± 0.14	2.35± 1.67	0.87
169	24.64 ± 0.19	27.52 ± 8.38	2.36± 4.08	3.26
217	24.16 ± 0.03	35.22 ± 0.34	4.27± 3.34	5.06
260	23.48± 0.04	9.52 ± 0.33	2.28± 1.64	3.29
328	22.71± 0.11	10.33± 0.04	1.58± 1.63	14.62
329	23.37± 0.03	5.15 ± 0.06	3.64± 4.76	3.59
350	22.92± 0.02	13.45 ± 0 02	2.66± 4.31	6.1
367	23.71± 0.03	15.76 ± 0.02	1.36± 3.46	1.78
381	24.11± 0.02	35.07± 0.07	3.19± 5.09	18.81
477	24.43± 0.03	15.87± 0.35	6.58± 3.92	13.86
530	23.48± 0.04	15.76 ± 0 .02	3.88± 1.21	23.06
565	23.47± 0.08	13,20± 1.47	3.47± 6.32	1.94
584	23.21 ± 0.01	9.67± 0.18	6.72 ± 2.89	4.86
826	22.75 ± 0.11	15.97± 0.05	4.91 ± 3.48	28.15
963	22.98 ± 0.08	6.83 ± 0 .02	4.00 ± 1.37	2.30
1013	23.08 ± 0.03	7.25± 0.13	1.11 ± 3.92	1.20
1455	22.38± 0.02	7.28 ± 0.10	5.44± 3.28	4.57
1465	23.21± 0.03	13.73± 0.12	2.34± 5.15	108.4
1468	22.47± 0.04	18.07± 0.15	1.95 ± 3.76	30.58
1585	23.00± 0.03	17.76 ± 0.20	3.21± 1.62	6.10
1753	22.86± 0.12	6.87± 0.13	6.51± 2.03	22.21
1784	24.48± 0.07	20.63± 0.12	2.37± 1.09	9.92
1816	23.55± 0.03	19.02± 0.38	5.93± 0.46	0.46
1822	22.74± 0.03	12.07± 0.08	2.34 ± 2.22	5.16
1952	23.55± 0.03	12.81± 0.06	1.28 ± 1.99	9.87
1992	23.09± 0.05	12.41± 0.23	1.36 ± 4.6	3.22

Note. — Reduced χ^2 statistics and fitting parameters to a buldge+disk profile $\mu = \mu_c + 1.086 \times (r/h) + 8.33 \times (r/r_e)^{1/4}$. μ_c is the B-central surface brightness in mag arcsec^{-2}, r_e is the B- effective radius of the central bulge, and h_B is the B- scale length of the outer disk in arcsec.

Table 4. Mean and median colors

VCC	$(U-B)$			$(B-V)$			$(V-R)$			$(R-I)$			N
	mean	σ	median	mean	σ	median	mean	σ	median	mean	σ	median	
17	-0.53	0.29	-0.57	0.44	0.23	0.49	0.24	0.19	0.22	0.55	0.23	0.63	46
83	···	···	···	0.72	0.30	0.59	0.51	0.19	0.54	0.45	0.15	0.45	36
168	-0.18	0.30	-0.17	0.76	0.42	0.76	0.43	0.14	0.41	0.52	0.12	0.48	13
169	-0.33	0.97	-0.51	-0.21	1.55	-0.31	0.19	1.55	0.39	0.94	0.77	0.77	46
217	0.08	0.33	0.09	0.62	0.13	0.62	-0.005	0.17	0.03	0.77	0.23	0.68	76
260	-0.40	0.11	-0.38	0.62	0.16	0.60	0.13	0.08	0.15	0.53	0.08	0.56	23
328	-0.48	0.26	-0.45	0.62	0.24	0.57	0.26	0.16	0.32	0.75	0.42	0.59	46
329	0.05	0.21	0.11	0.40	0.19	0.41	0.50	0.30	0.40	0.12	0.17	0.11	16
350	···	···	···	0.40	0.13	0.39	0.41	0.12	0.44	0.43	0.22	0.43	36
367	1.07	0.44	1.24	1.01	0.08	0.99	0.31	0.11	0.35	0.74	0.06	0.71	36
381	0.08	0.30	0.09	0.38	0.15	0.37	0.12	0.33	0.12	0.92	0.38	0.81	31
477	0.27	0.33	0.29	0.52	0.15	0.52	0.11	0.17	0.12	0.18	0.52	0.32	33
530	0.64	0.12	0.66	0.44	0.16	0.48	0.41	0.18	0.41	0.56	0.13	0.55	60
565	-0.07	0.23	-0.13	0.60	0.21	0.54	0.37	0.14	0.42	0.48	0.11	0.45	16
584	-0.44	0.31	-0.45	0.09	0.17	0.09	0.86	0.13	0.87	0.41	0.18	0.41	27
826	0.03	0.28	-0.07	0.03	0.11	0.05	0.53	0.17	0.51	-0.01	0.16	-0.03	57
963	-0.26	0.20	-0.26	0.50	0.10	0.49	0.36	0.04	0.37	0.36	0.13	0.40	21
1013	···	···	···	0.56	0.27	0.53	0.62	0.19	0.62	0.64	0.21	0.57	26
1455	-0.10	0.16	-0.06	0.55	0.08	0.53	0.48	0.20	0.57	0.33	4.E-5	0.33	29
1465	0.39	0.63	0.30	0.67	0.09	0.65	0.56	0.20	0.50	-0.31	0.95	0.13	46
1468	0.55	0.34	0.46	0.57	0.03	0.57	0.33	0.05	0.31	0.55	0.02	0.55	25
1585	-0.002	0.21	-0.005	0.24	0.25	0.32	0.80	0.27	0.82	0.11	0.25	0.18	47
1753	-0.48	0.27	-0.48	0.33	0.26	0.24	0.23	0.33	0.32	-0.08	0.46	-0.002	23
1784	-0.36	0.40	-0.47	0.33	0.11	0.32	0.39	0.08	0.40	0.64	0.07	0.66	44
1816	-0.23	0.19	-0.18	0.10	0.17	0.11	0.91	0.09	0.94	0.37	0.06	0.40	15
1822	-0.05	0.30	-0.11	0.47	0.09	0.47	0.19	0.08	0.21	0.44	0.15	0.39	46
1952	-0.42	0.20	-0.44	0.60	0.09	0.59	0.36	0.09	0.38	0.22	0.30	0.34	31
1992	-0.50	0.39	-0.58	0.45	0.16	0.44	0.08	0.05	0.09	0.04	0.22	0.08	11

Note. — σ is the standard deviation of the values and N is the number of data points along the radius.

Table 5. Color gradients

VCC	Δ_{U-B} (χ^2)	Δ_{B-V} (χ^2)	Δ_{V-R} (χ^2)	Δ_{R-I} (χ^2)	h_B
17	-0.006 ± 0.001 (5.79)	6.0E-4 ± 0.001 (1.50)	1.9E-4 ± 0.001 (1.20)	-0.004 ± 0.001 (1.90)	25.73
83	···	0.008 ±0.001 (2.00)	0.007 ± 4.E-4 (8.90)	-0.006 ± 5.E-4 (3.40)	10.64
168	-0.110 ± 0.030 (4.42)	0.120 ± 0.020 (1.80)	-0.043 ± 0.007 (0.97)	0.030 ± 0.006 (3.96)	6.26
169	0.005 ± 0.017 (4.13)	-0.006 ± 0.006 (5.70)	-0.019 ± 0.007 (26.08)	-0.027 ± 0.050 (4.58)	29.52
217	0.003 ± 0.001 (4.56)	-0.004 ±4.E-4 (3.90)	-0.006 ± 5.E-4 (2.90)	0.009 ± 5.E-4 (4.10)	38.67
260	0.008 ± 0.035 (2.95)	0.014 ± 0.003 (2.39)	-0.004 ± 0.002 (0.71)	-0.003 ± 0.002 (2.36)	13.68
328	-0.008 ± 0.001 (4.10)	0.012 ±7.E-4 (2.97)	0.0013 ± 5.E-4 (2.92)	0.034 ± 6.E-4 (12.80)	14.44
329	-0.029 ± 0.014 (3.44)	0.011 ± 0.007 (3.05)	0.036 ± 0.008 (2.58)	0.002 ± 0.011 (2.36)	7.84
350	···	0.001 ± 0.003 (2.33)	0.016 ± 0.003 (0.52)	0.021 ± 0.002 (2.21)	12.88
367	···	0.008 ± 0.001 (1.12)	-0.010 ± 8.E-4 (2.11)	0.005 ± 8.E-4 (0.95)	14.48
381	-0.035 ± 0.002 (3.93)	0.006 ± 0.002 (4.22)	-0.003 ± 0.003 (3.59)	-0.005 ± 0.004 (4.13)	25.88
477	-0.023 ± 0.006 (4.20)	0.003 ± 0.002 (2.69)	0.001 ± 0.003 (1.83)	-0.004 ± 0.005 (2.11)	20.58
530	0.006 ± 0.006 (2.95)	-0.004 ± 3.E-4 (5.53)	0.011 ± 3.E-4 (5.52)	0.008 ± 1.E-4 (4.94)	6.43
565	0.043 ± 0.017 (2,07)	-0.019 ± 0.005 (3.81)	-0.002 ± 0.005 (3.38)	0.010 ± 0.005 (2.11)	15.51
584	-0.074 ± 0.033 (1.88)	0.012 ± 0.040 (2.31)	0.014 ± 0.003 (1.51)	0.007 ± 0.005 (1.29)	6.10
826	0.007 ± 0.001 (3.60)	-7.E-4 ± 0.001 (0.71)	0.004 ± 0.001 (1.38)	-0.004 ± 0.002 (1.41)	21.04
963	-0.024 ± 0.003 (4.93)	0.005 ± 0.002 (6.33)	0.004 ± 0.001 (5.10)	-0.002 ± 0.002 (9.13)	6.49
1013	···	-0.003 ± 0.003 (1.35)	0.011 ± 0.002 (3.11)	0.012 ± 0.001 (4.78)	9.76
1455	-0.007 ± 0.002 (8.62)	0.008 ± 0.001 (1.98)	-0.007 ± 0.002 (4.13)	-1.E-5 ± 0.001 (0.10)	8.11
1465	-0.013 ± 0.003 (2.69)	-2.E-4 ± 5.E-4 (5.41)	0.015 ± 5.E-4 (10.01)	-0.037 ± 7.E-4 (35.0)	20.91
1468	-0.023 ± 0.010 (2.62)	-0.001 ± 8.E-4 (0.71)	1.E-5 ± 8.E-4 (3.33)	0.001 ± 6.E-4 (0.86)	23.75
1585	-0.009 ± 0.002 (2.00)	-0.019 ± 0.002 (1.21)	0.024 ± 0.001 (0.61)	-0.014 ± 0.002 (0.47)	22.49
1753	-0.019 ± 0.004 (3.91)	0.021 ± 0.002 (1.46)	0.001 ± 0.007 (1.81)	0.009 ± 0.013 (2.03)	10.57
1784	-0.026 ± 0.002 (2.77)	-0.002 ± 3.E-4 (2.52)	4.E-5 ± 3.E-5 (3.89)	-0.005 ± 3.E-4 (2.30)	26.11
1816	0.020 ± 0.006 (0.42)	0.016 ± 0.005 (0.27)	0.012 ± 0.006 (0.58)	5.E-4 ± 0.005 (0.41)	18.60
1822	0.022 ± 0.001 (4.12)	0.006 ± 5.E-4 (2.18)	-0.002 ± 7.E-4 (2.89)	0.009 ± 0.001 (4.39)	14.82
1952	0.025± 0.004 (1.11)	-0.006 ± 6.E-4 (2.40)	-0.002 ± 7.E-4 (1.96)	-0.004 ± 8.E-4 (4.58)	16.65
1992	-0.052 ± 0.005 (0.91)	-0.016 ± 0.004 (0.44)	-0.004 ± 0.006 (0.08)	-0.017 ± 0.011 (0.13)	23.06

Note. — Color gradients derived from weighted linear fit, $(color) = (color)_\circ + \Delta_{color} \times r$, where Δ_{color} is the gradient per arcsec. h_B is the B-band scale length in arcsec.

Table 6. Color indices of common galaxies in the Virgo cluster derived by other authors

VCC	$(U-B)$	$(B-V)$	$(V-R)$	$(R-I)$	$(V-I)$	reference	aperture
VCC 17	···	0.46	···	···	0.18	BMCM	ellip. 6
	···	0.38	···	···	0.09	BMCM	ellip. 38
	···	0.58± 0.04	0.23±0.07	0.57±0.05	0.80 ±0.09	A&B	poly.
VCC 83	···	0.61±0.03	0.53±0.07	0.54±0.05	1.07 ±0.05	A&B	poly.
VCC 168	···	0.76±0.17	0.62 ±0.10	0.29±0.09	0.91±0.13	A&B	poly.
VCC 260	···	0.47 ±0.05	0.41±0.08	0.41±0.06	0.82±0.10	A&B	poly.
VCC 328	···	0.39	···	···	0.05	BMCM	ellip. 6
	···	0.40	···	···	0.12	BMCM	ellip. 33
	-0.37± 0.10	0.67 ± 0.10	···	···	···	G&H	circ. 10
VCC 381	-0.20 ± 0.20	0.00 ± 0.20	···	···	···	G&H	circ. 30
VCC 530	···	0.51	···	···	0.08	BMCM	ellip. 6
	···	0.46	···	···	0.04	BMCM	ellip. 23
VCC 565	···	0.53±0.06	0.45±0.05	0.43±0.04	0.88±0.06	A&B	poly.
VCC 1013	···	0.52±0.05	0.40±0.10	0.45±0.03	0.85±0.11	A&B	poly.
VCC 1468	···	0.54±0.05	0.24±0.03	-0.25±0.21	-0.01±0.21	A&B	poly.
VCC 1585	···	0.53	···	···	0.13	BMCM	ellip. 6
	···	0.46	···	···	0.09	BMCM	ellip. 58
	-0.22± 0.04	0.43 ± 0.05	···	···	···	G&H	circ. 50
VCC 1952	···	0.63±0.03	0.40±0.02	0.31±0.03	0.71±0.04	A&B	poly.
VCC 1992	···	0.43	···	···	0.20	BMCM	ellip. 6
	···	0.35	···	···	0.08	BMCM	ellip. 30
	-0.22 ± 0.06	0.41 ± 0.06	···	···	···	G&H	circ. 6

Note. — The circular (G&H) or elliptical (BMVM) radius-aperture is in arcsec units. The guideline for setting the border of the polygon area (A&B) is that the signal-to noise ratio for each pixel of the object's image fall well bellow unity. BMCM list an average uncertainly of 0.03mag for the colors.

Fig. 1.— Profile fitting models. Dot-dashed line represent $\mu = \mu_\circ + 1.086 \times (r/h)^n$, dashed line is $\mu = \mu_\circ + 1.086 \times (r/h)$, solid line is $\mu = \mu_e + 8.33 \times ((r/R_e)^{1/4} - 1)$, and dotted line is $\mu = \mu_c\ 1.086 \times (r/h) + 8.33 \times (r/R_e)^{1/4}$

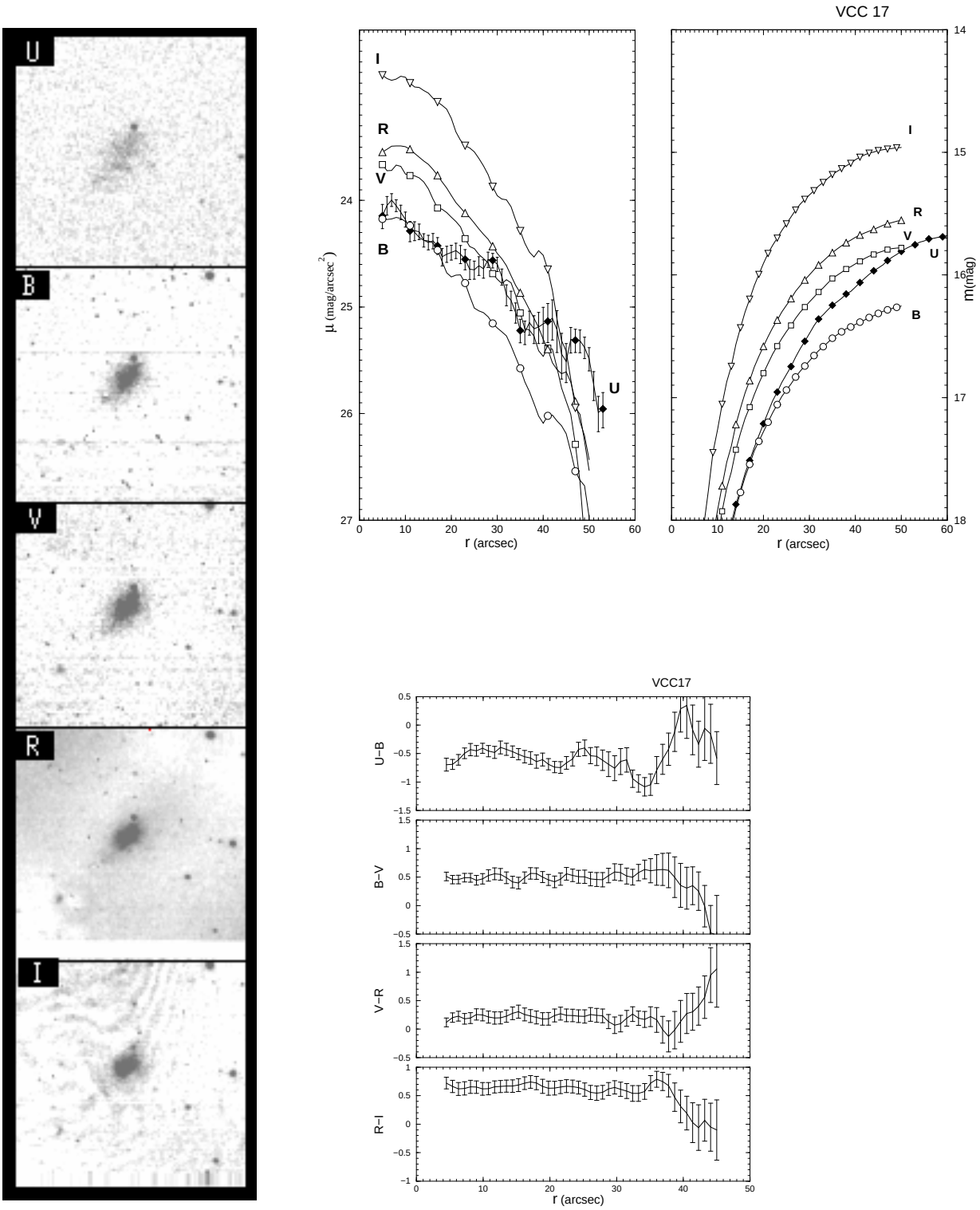

Fig. 2.— VCC 17- UBVRI images, μ is the surface brightness in $mag/arcsec^2$, and m the integrated magnitud at the aperture r (semi-major axis of the ellipse in $arcsec$). The color indexes are in $mag/arcsec^2$. Symbols represents: fill-diamonds for U, circles for B, squares for V, triangles-up for R, triangles-down for I.

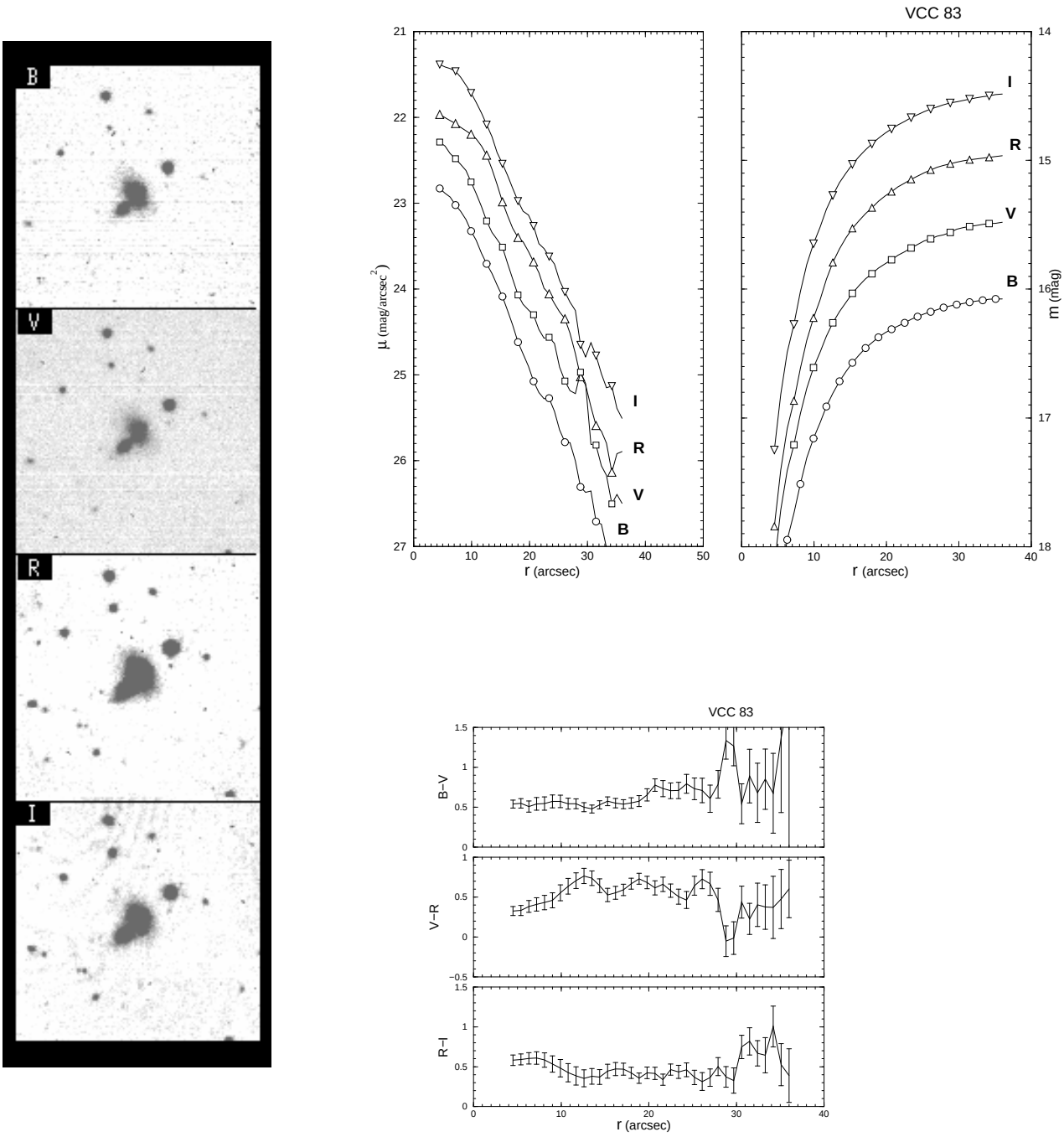

Fig. 3.— VCC 83- Symbols as in Fig. 2

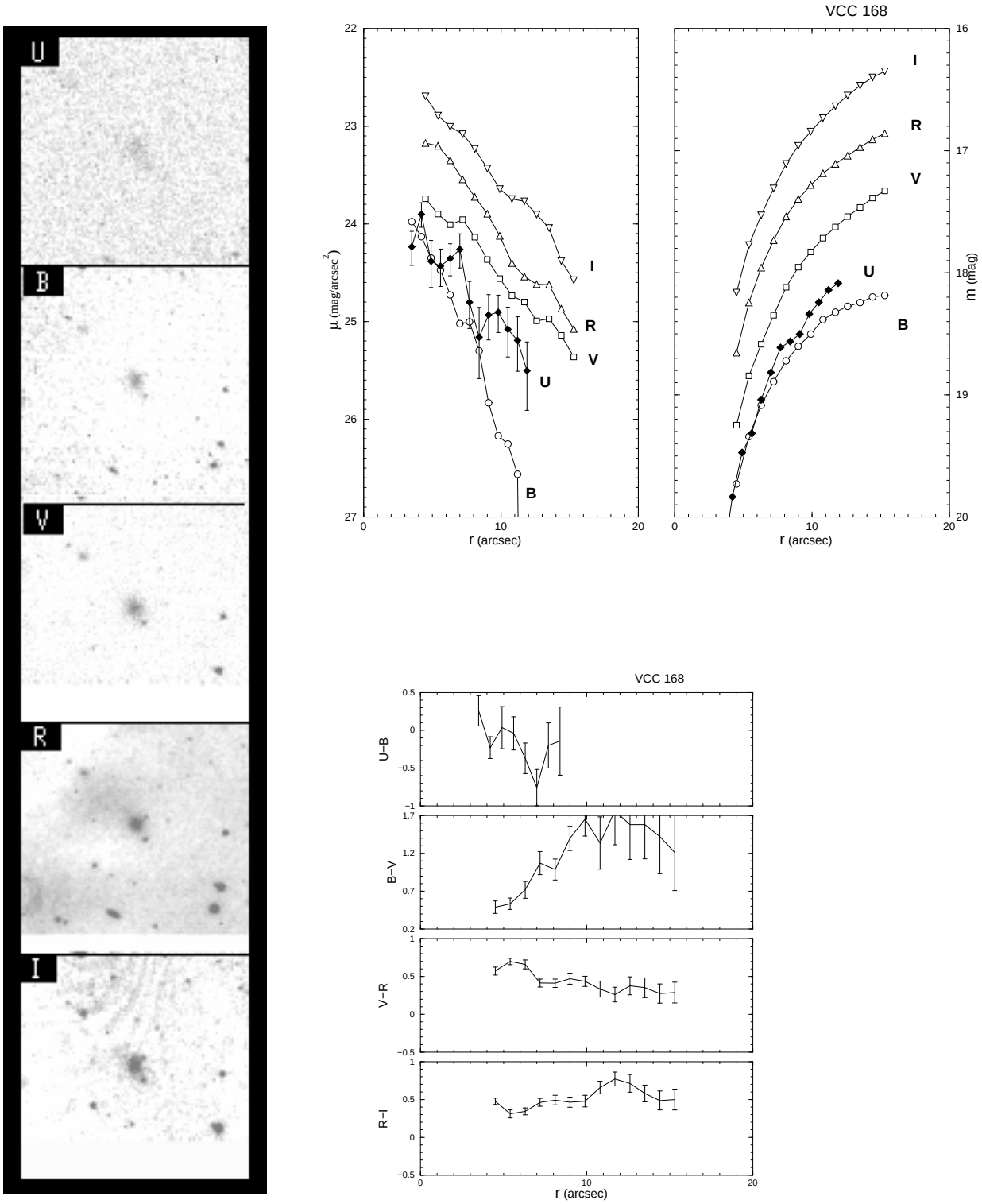

Fig. 4.— VCC 168- Symbols as in Fig. 2

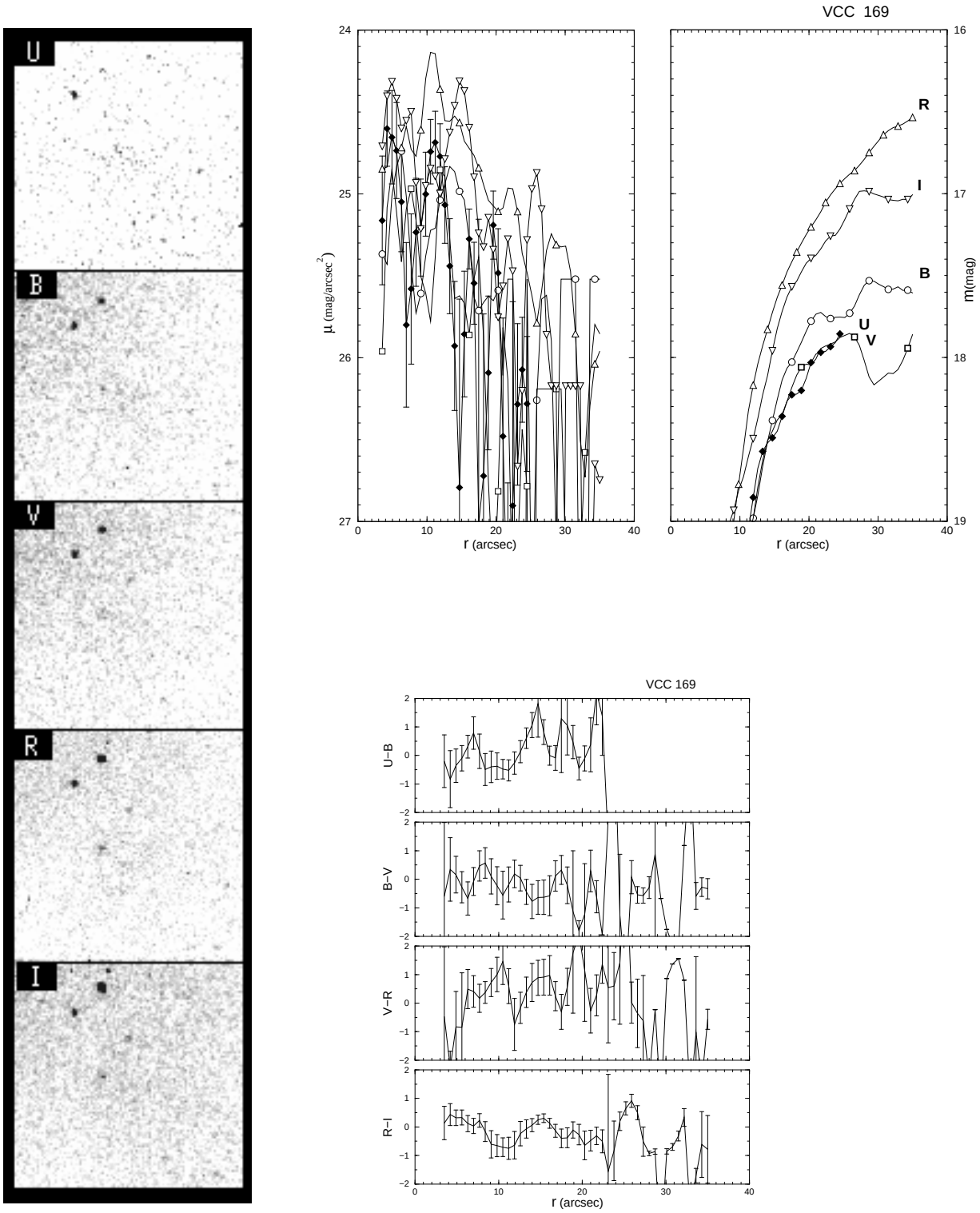

Fig. 5.— VCC 169- Symbols as in Fig 2. Very uncertain photometric results due to low S/N in all the images.

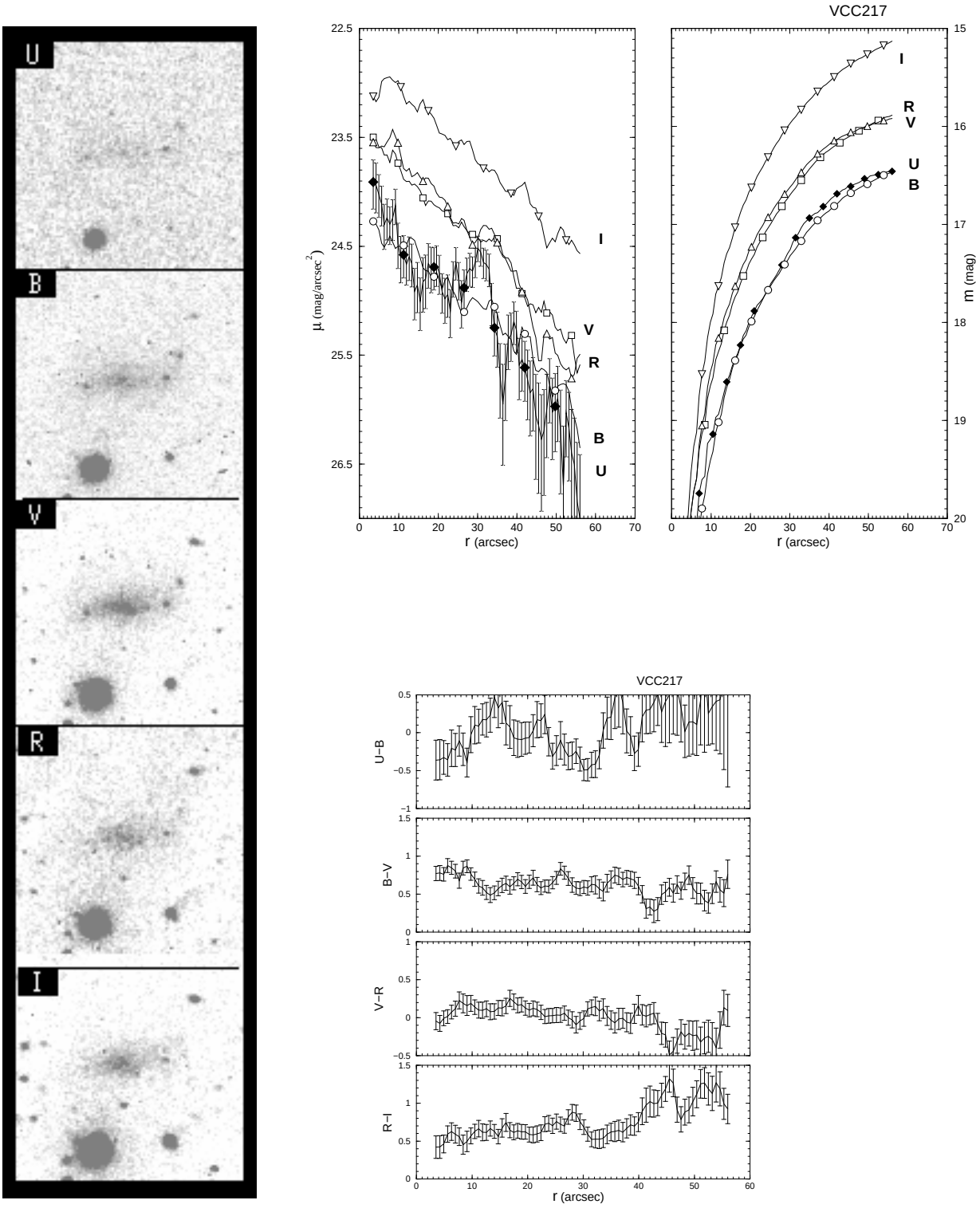

Fig. 6.— VCC 217- Symbols as in Fig. 2

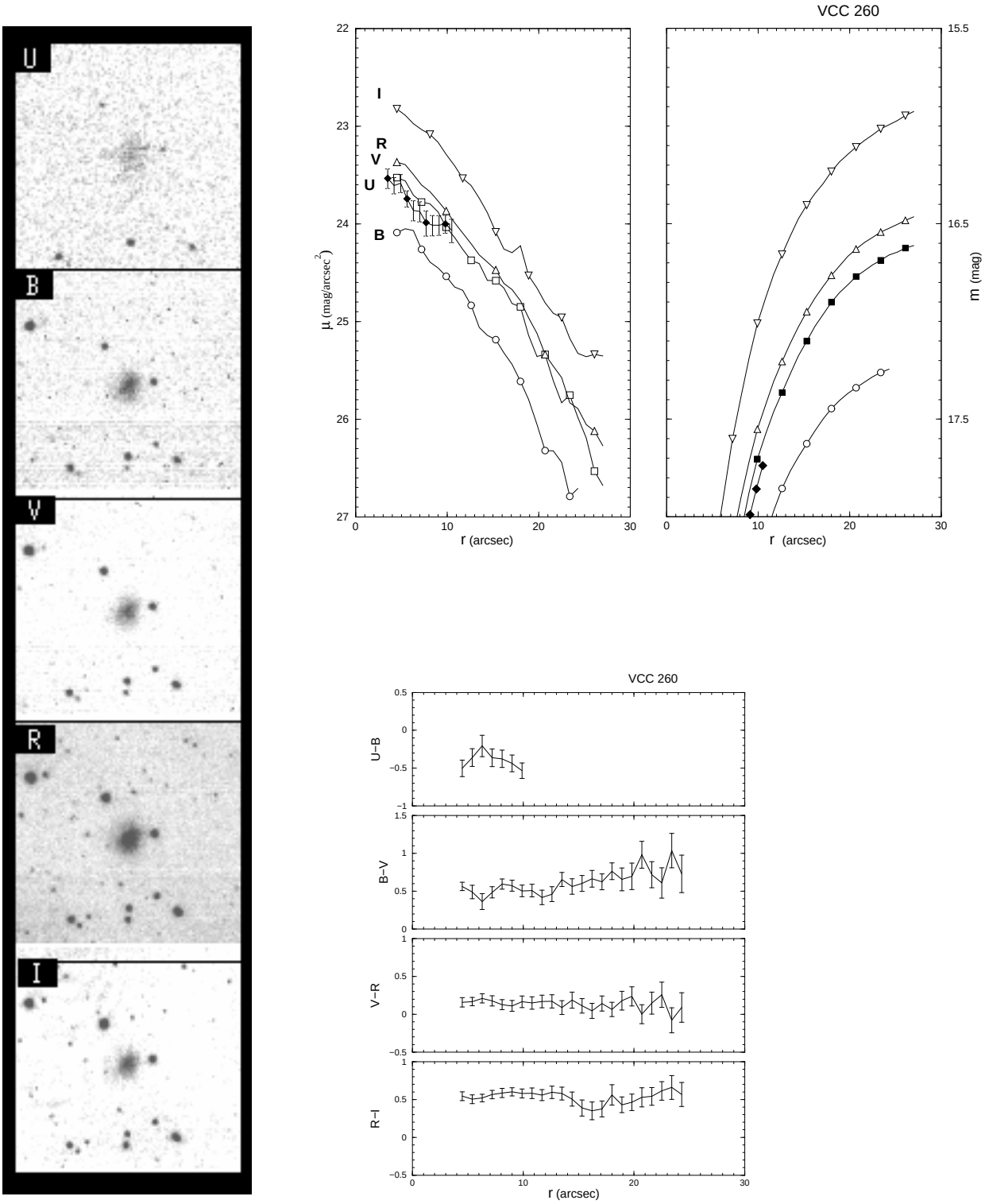

Fig. 7.— VCC 260- Symbols as in Fig. 2

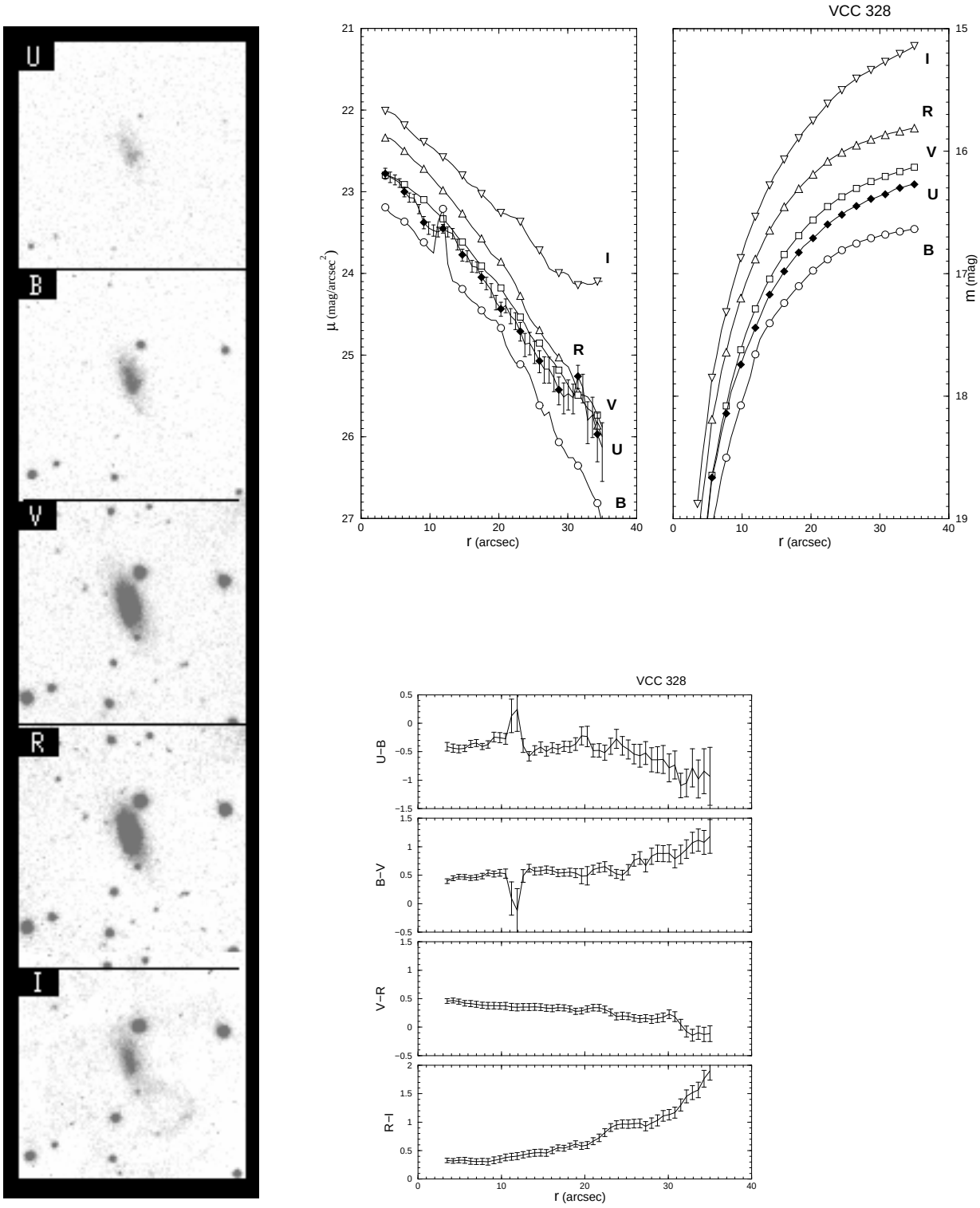

Fig. 8.— VCC 328- Symbols as in Fig. 2

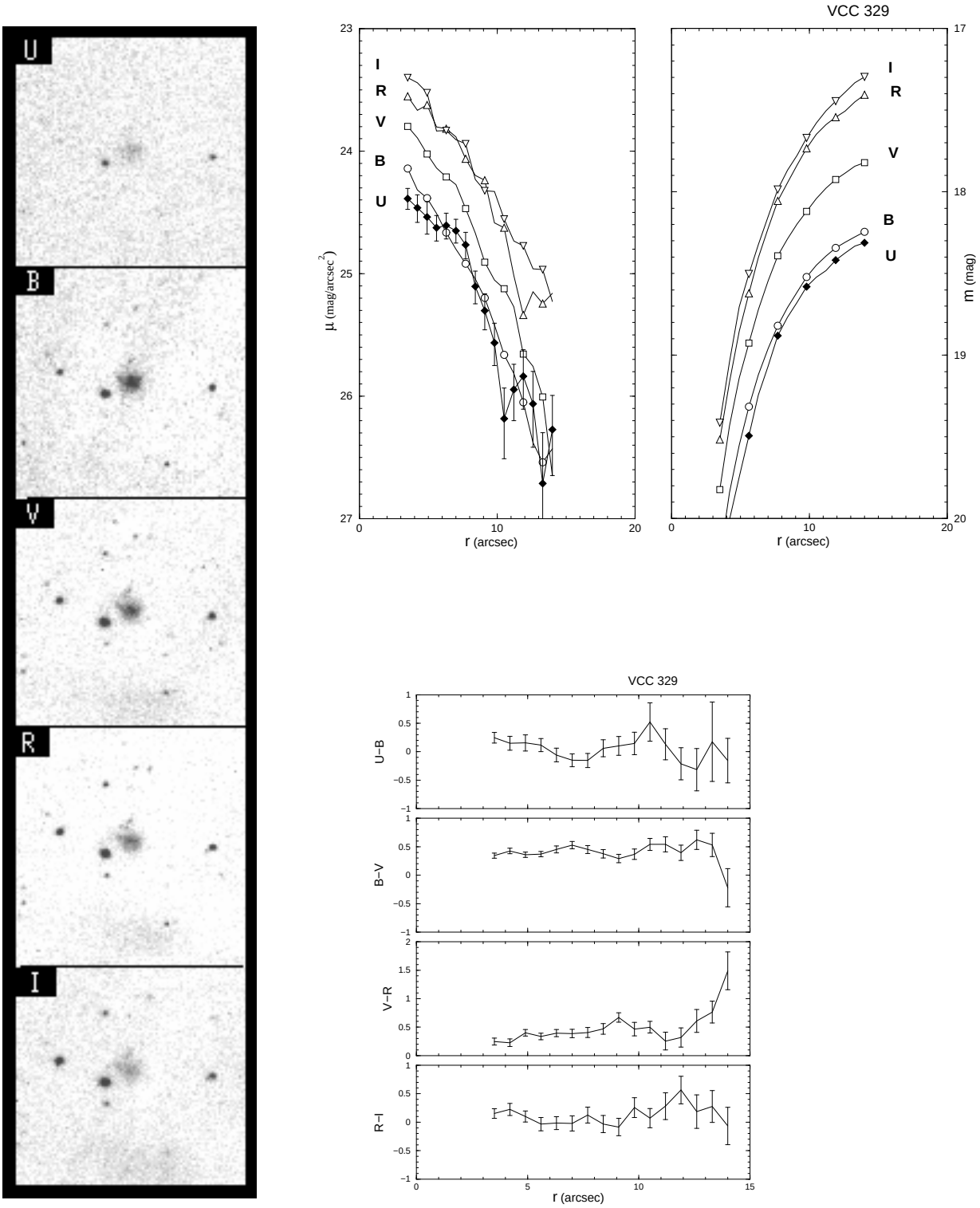

Fig. 9.— VCC 329- Symbols as in Fig. 2

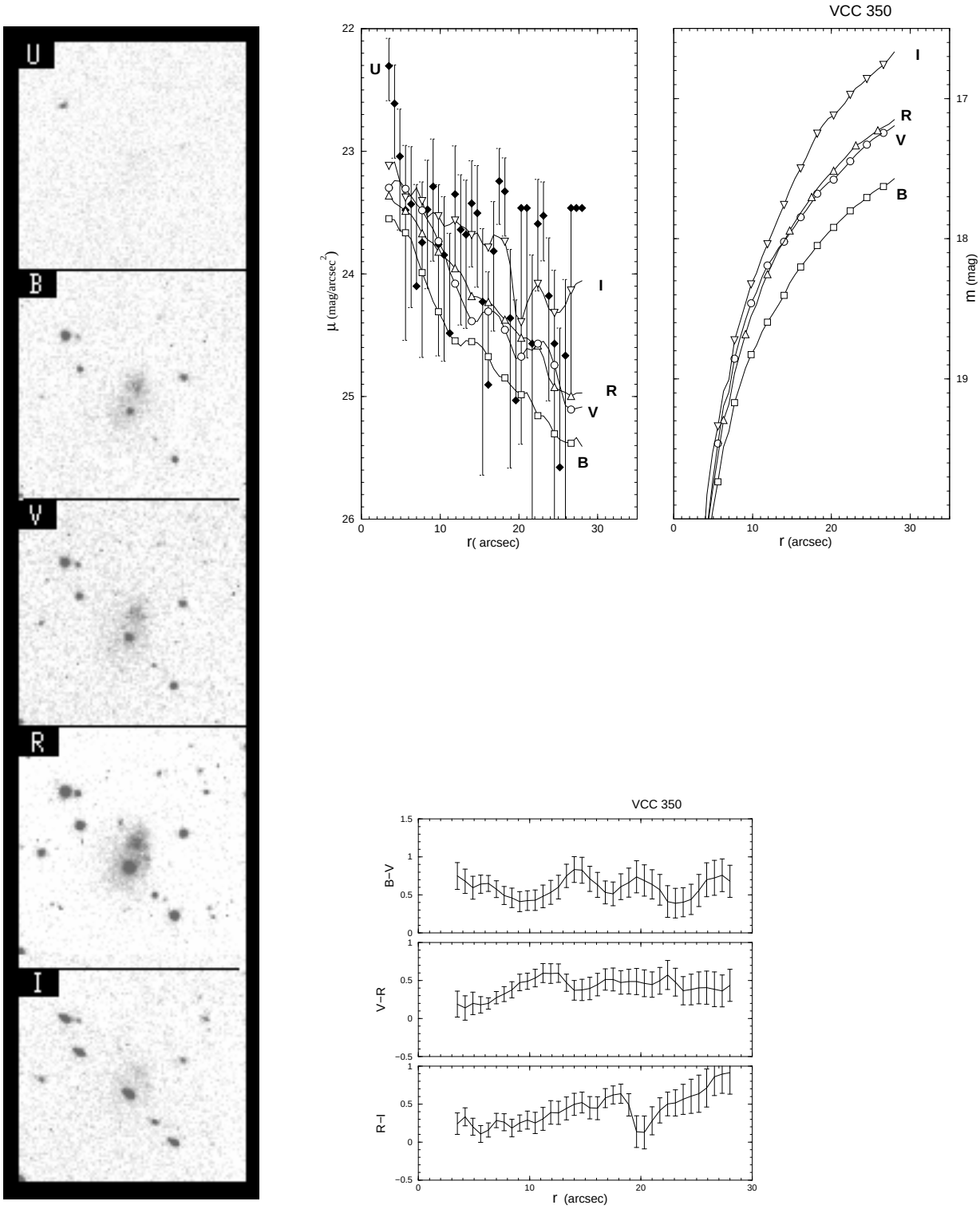

Fig. 10.— VCC 350- Symbols as in Fig. 2

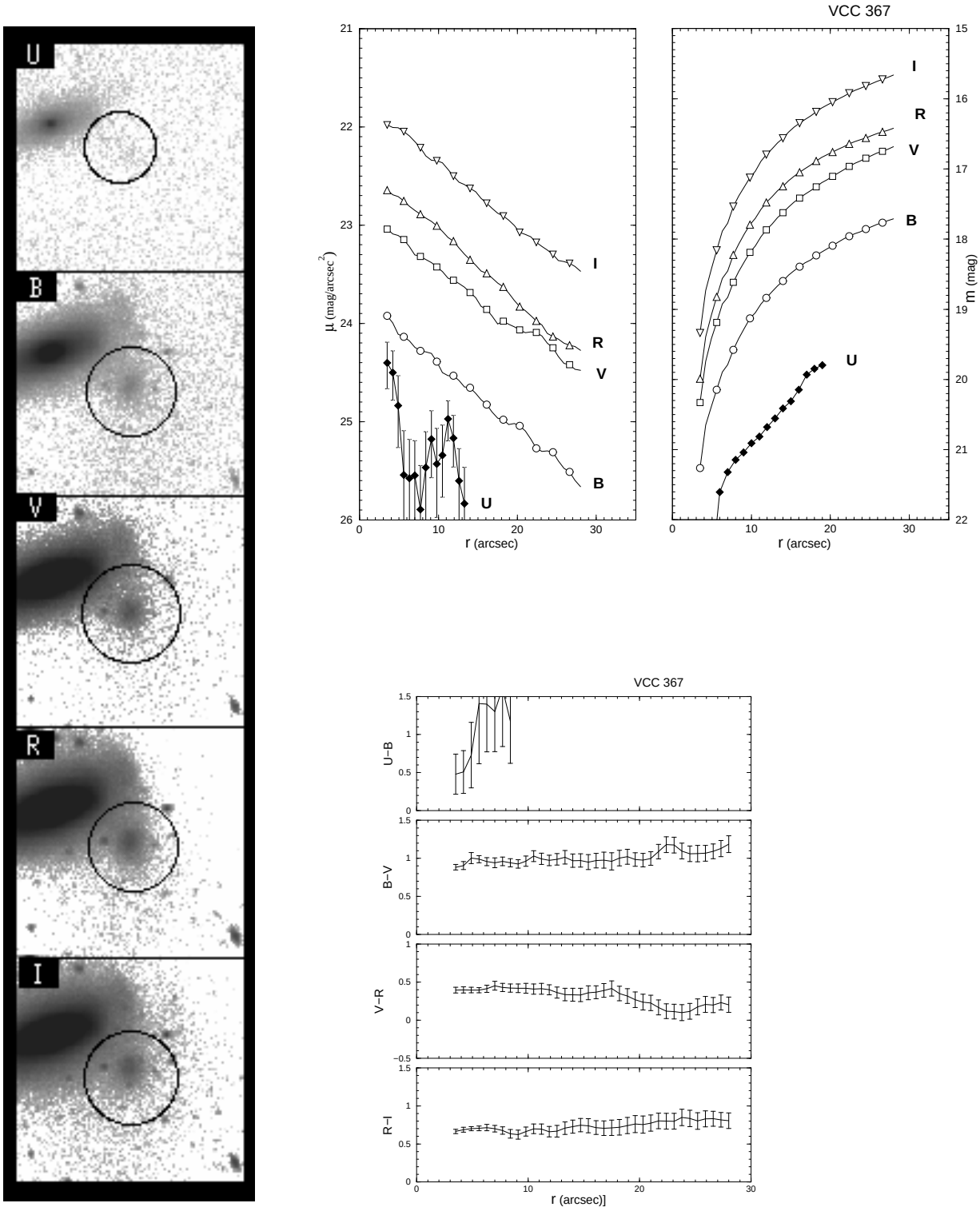

Fig. 11.— VCC 367- Symbols as in Fig. 2

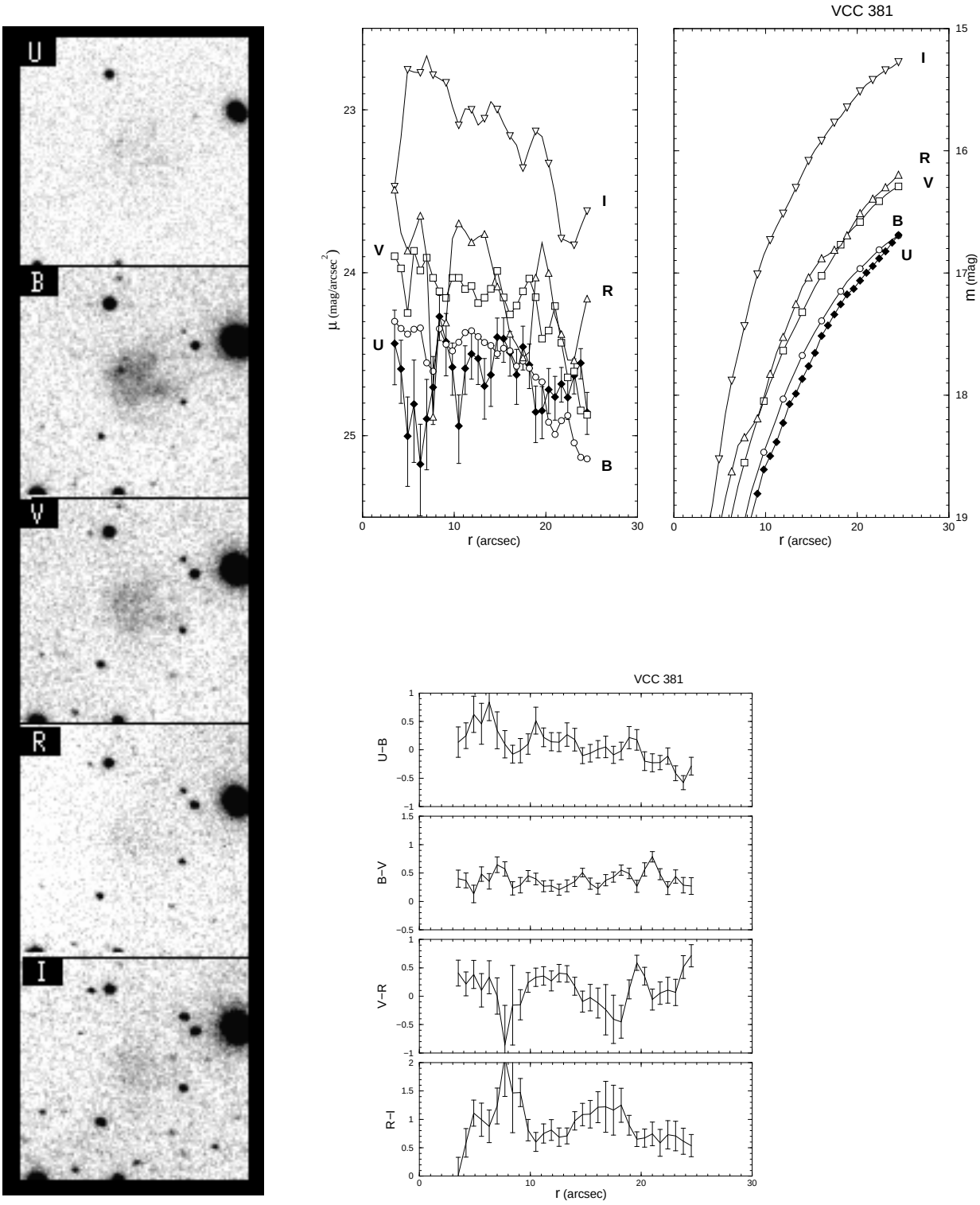

Fig. 12.— VCC 381- Symbols as in Fig. 2

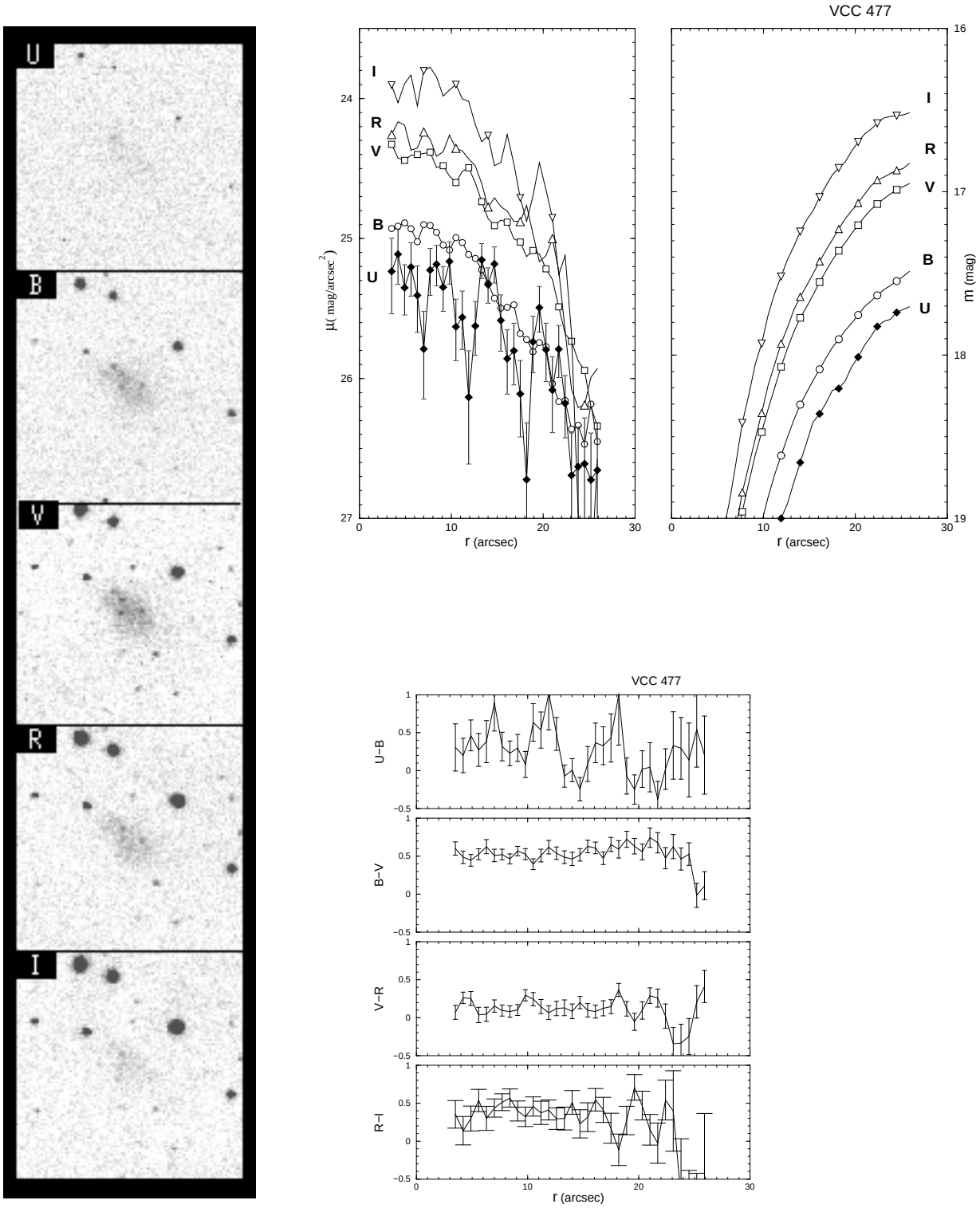

Fig. 13.— VCC 477- Symbols as in Fig. 2

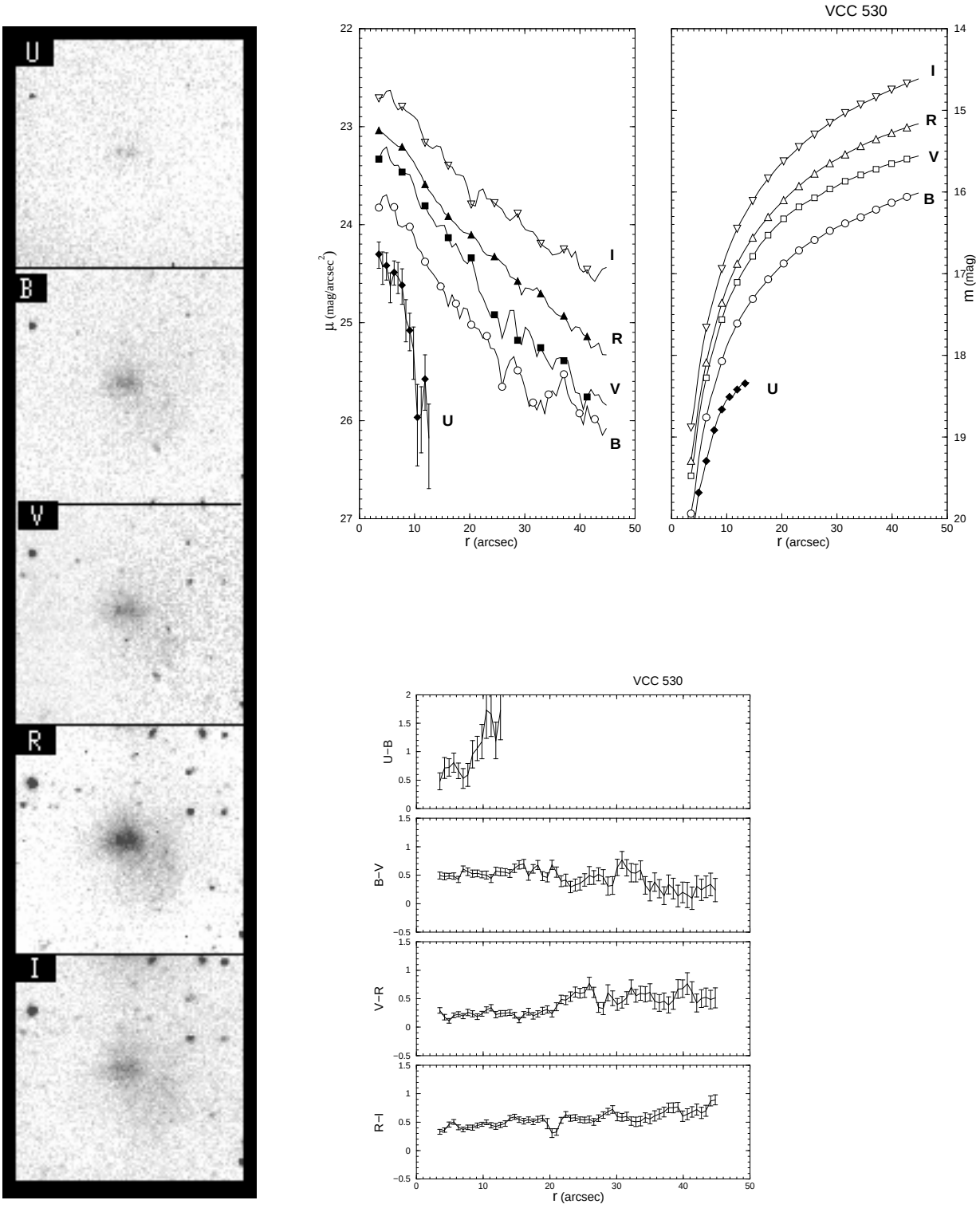

Fig. 14.— VCC 530- Symbols as in Fig. 2

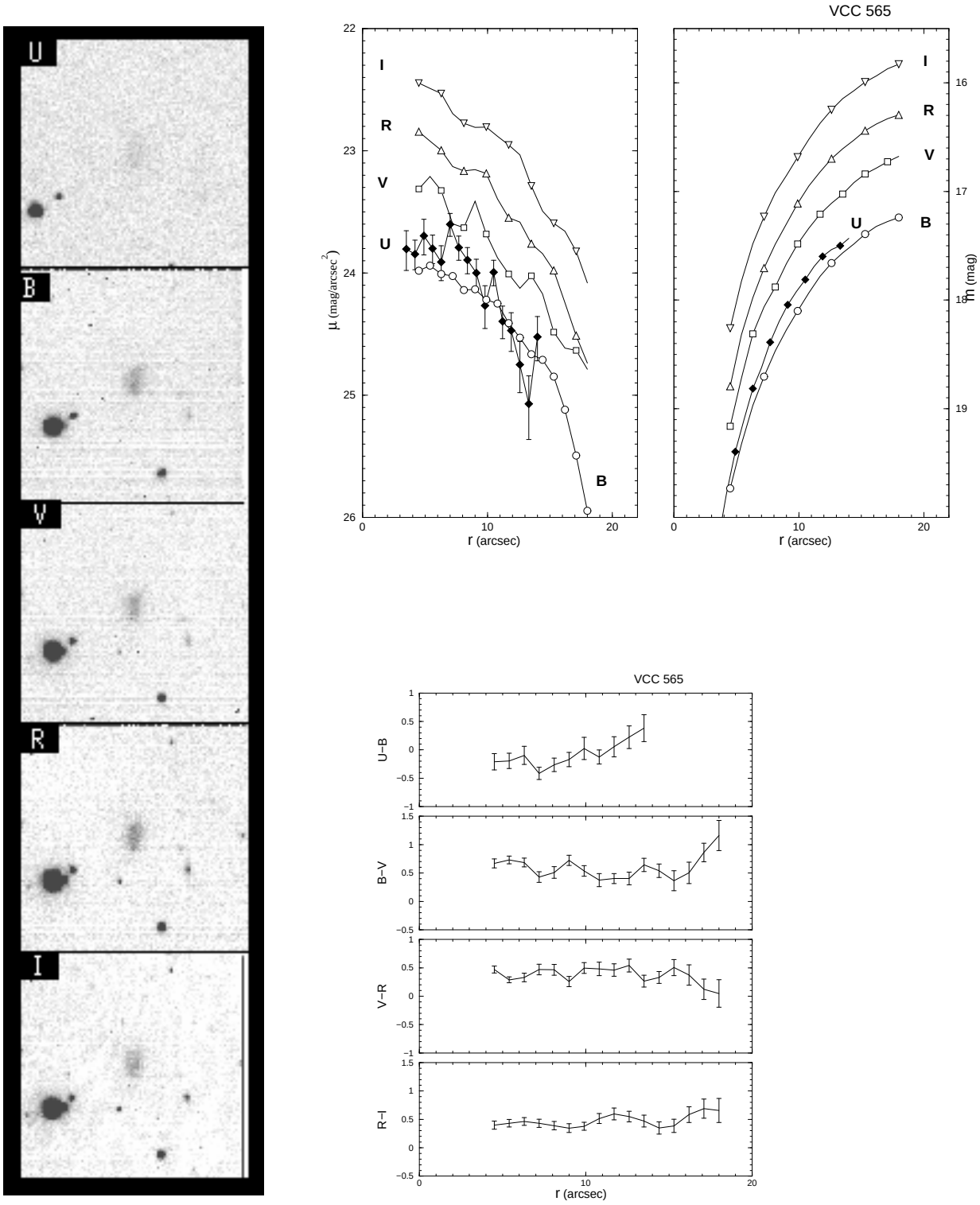

Fig. 15.— VCC 565- Symbols as in Fig. 2

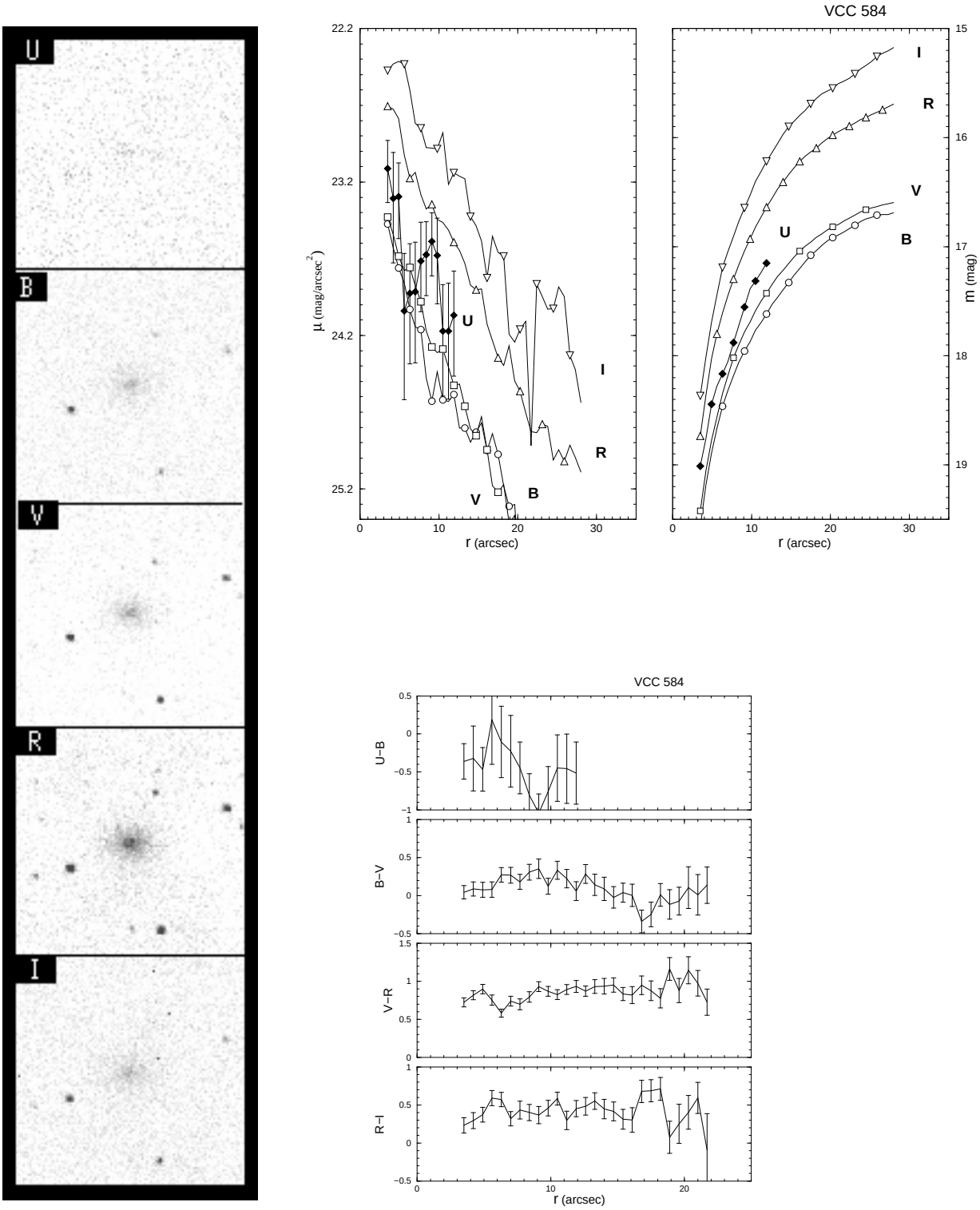

Fig. 16.— VCC 584- Symbols as in Fig. 2

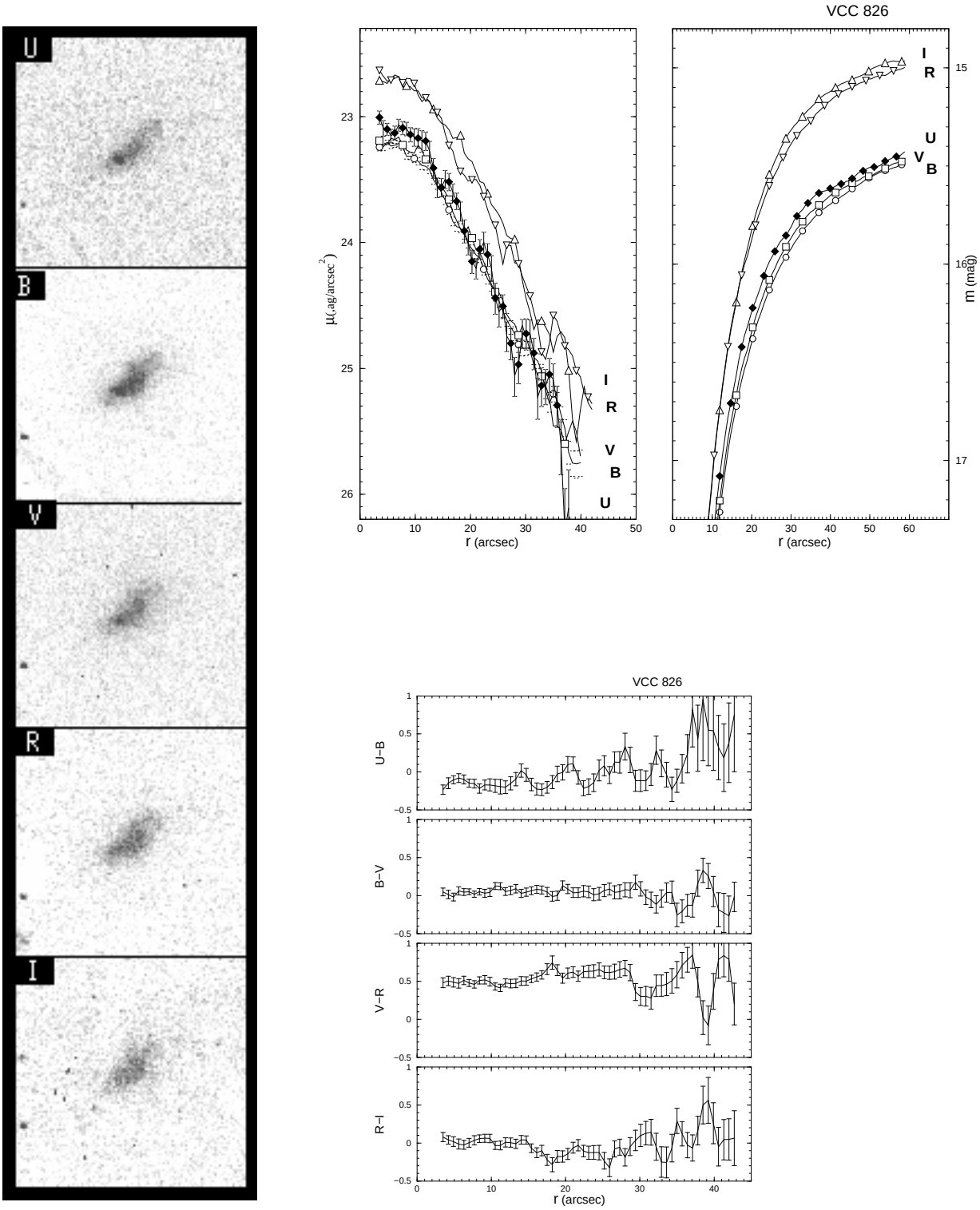

Fig. 17.— VCC 826- Symbols as in Fig. 2

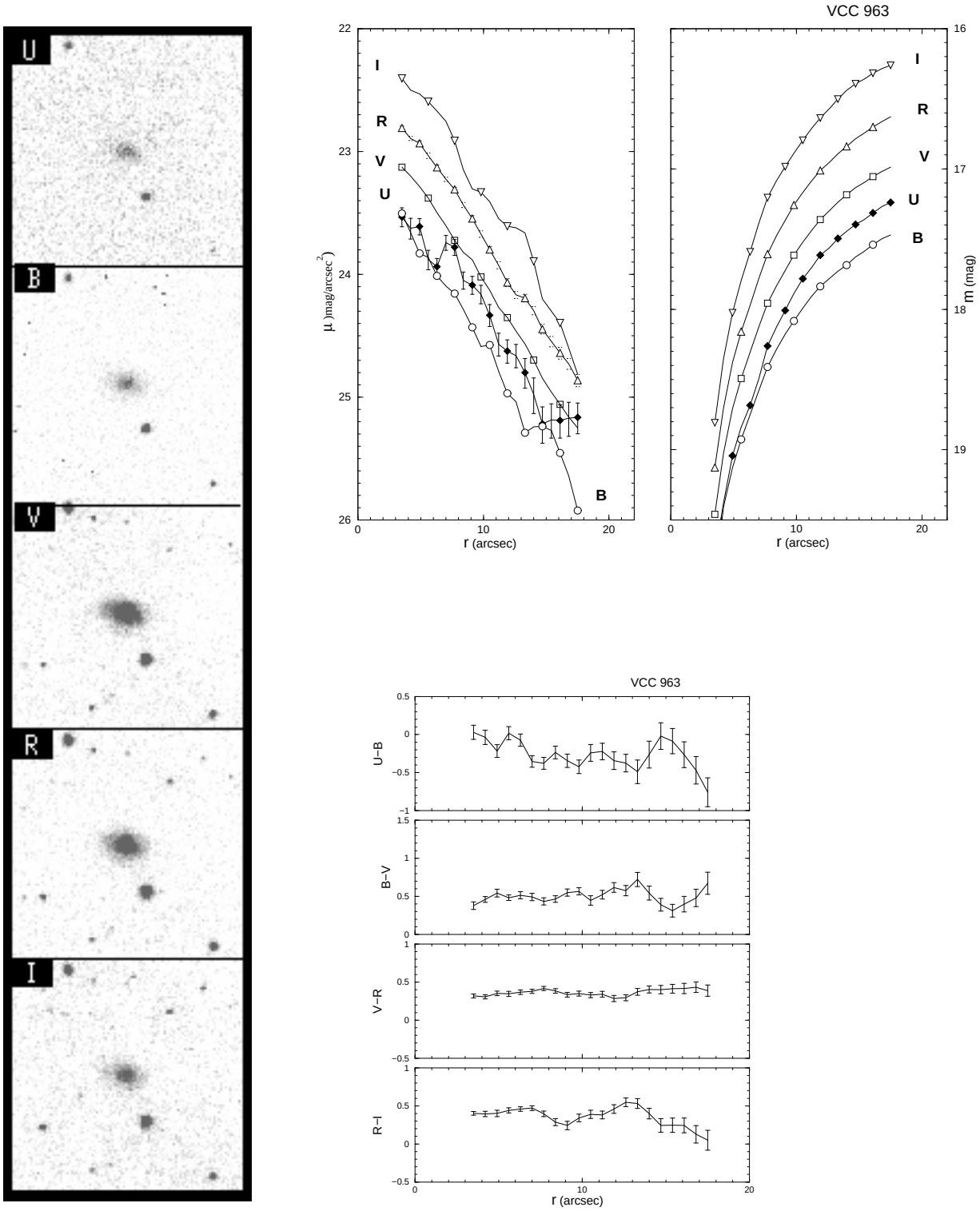

Fig. 18.— VCC 963- Symbols as in Fig. 2

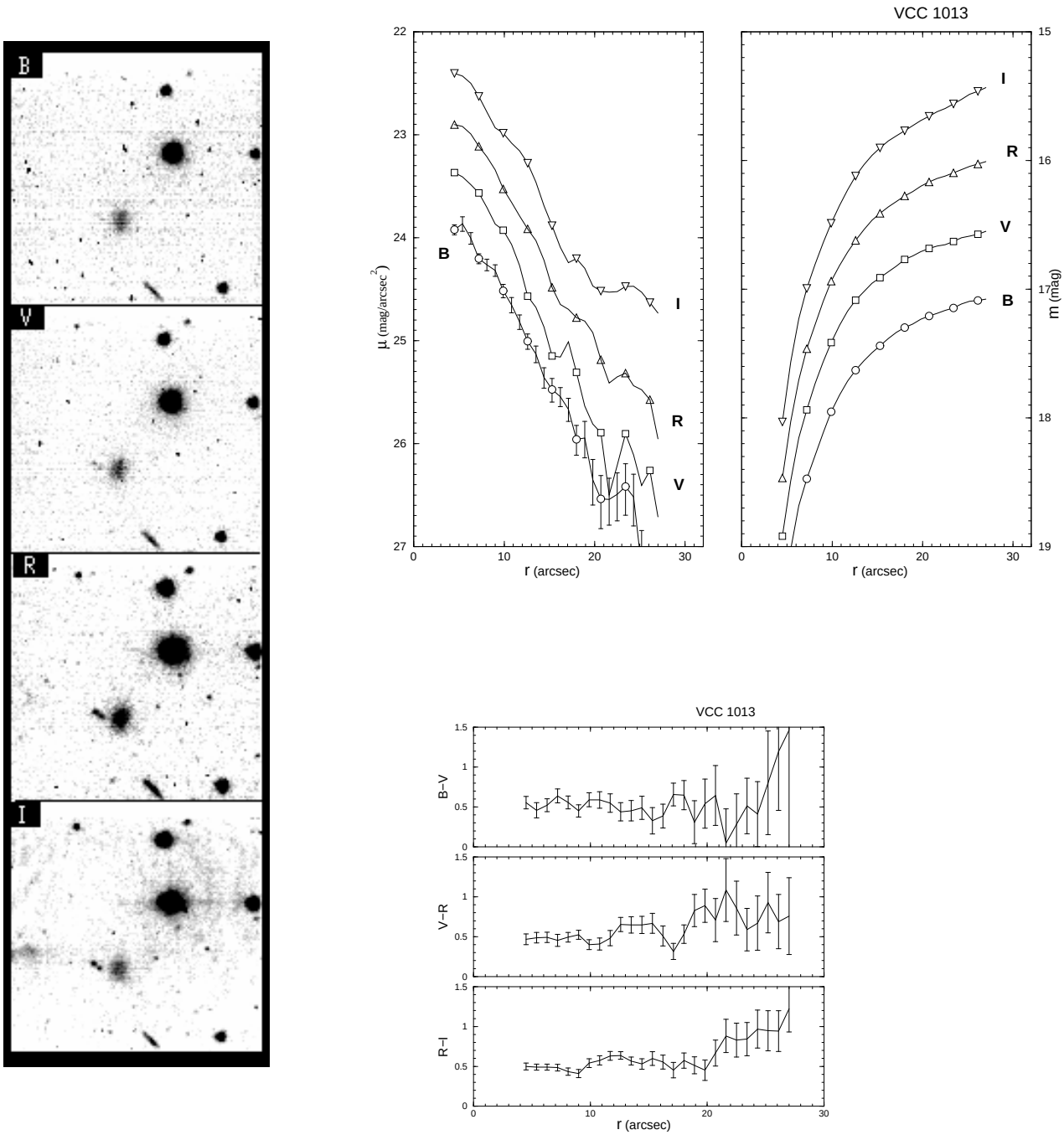

Fig. 19.— VCC 1013- Symbols as in Fig. 2

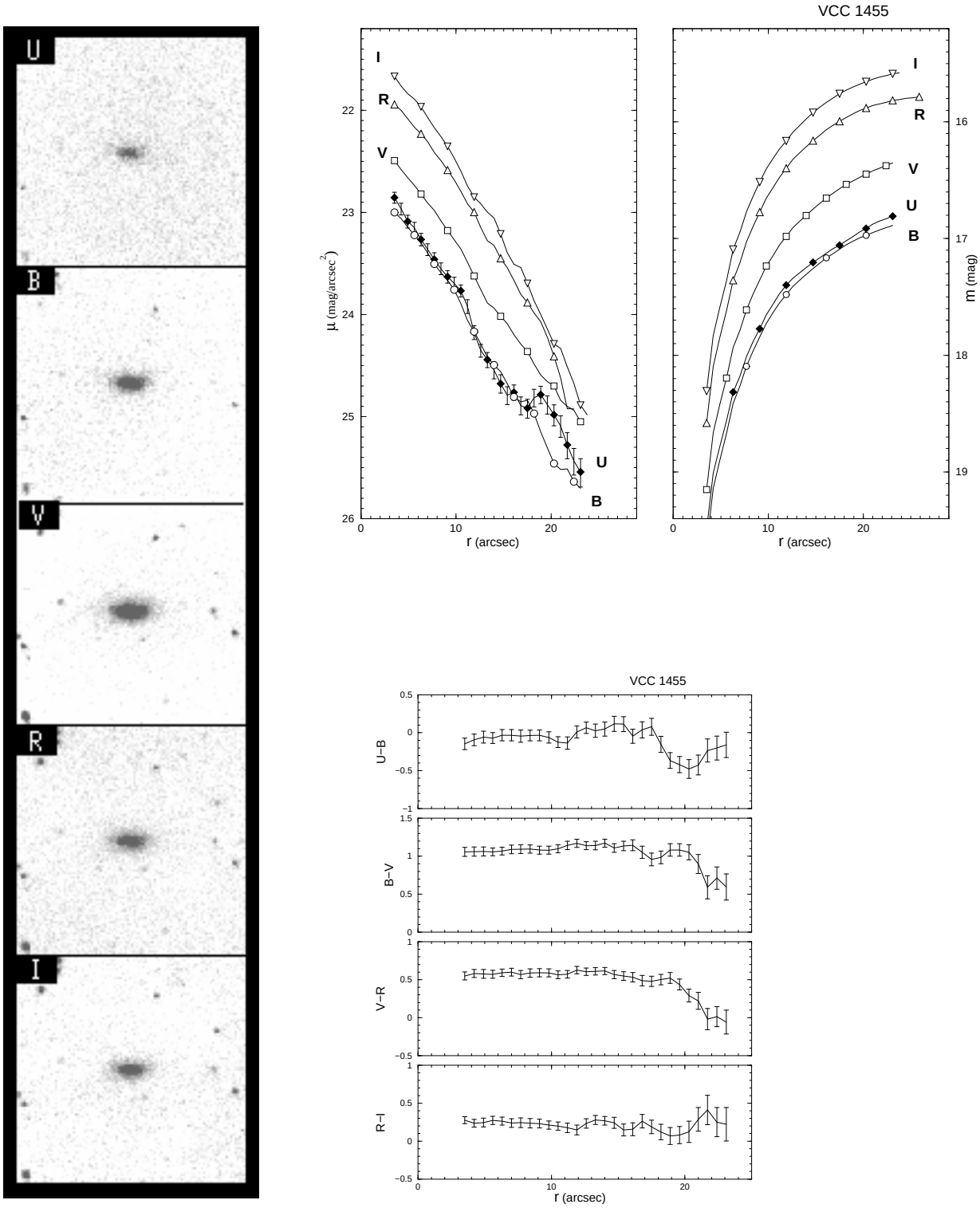

Fig. 20.— VCC 1455- Symbols as in Fig. 2

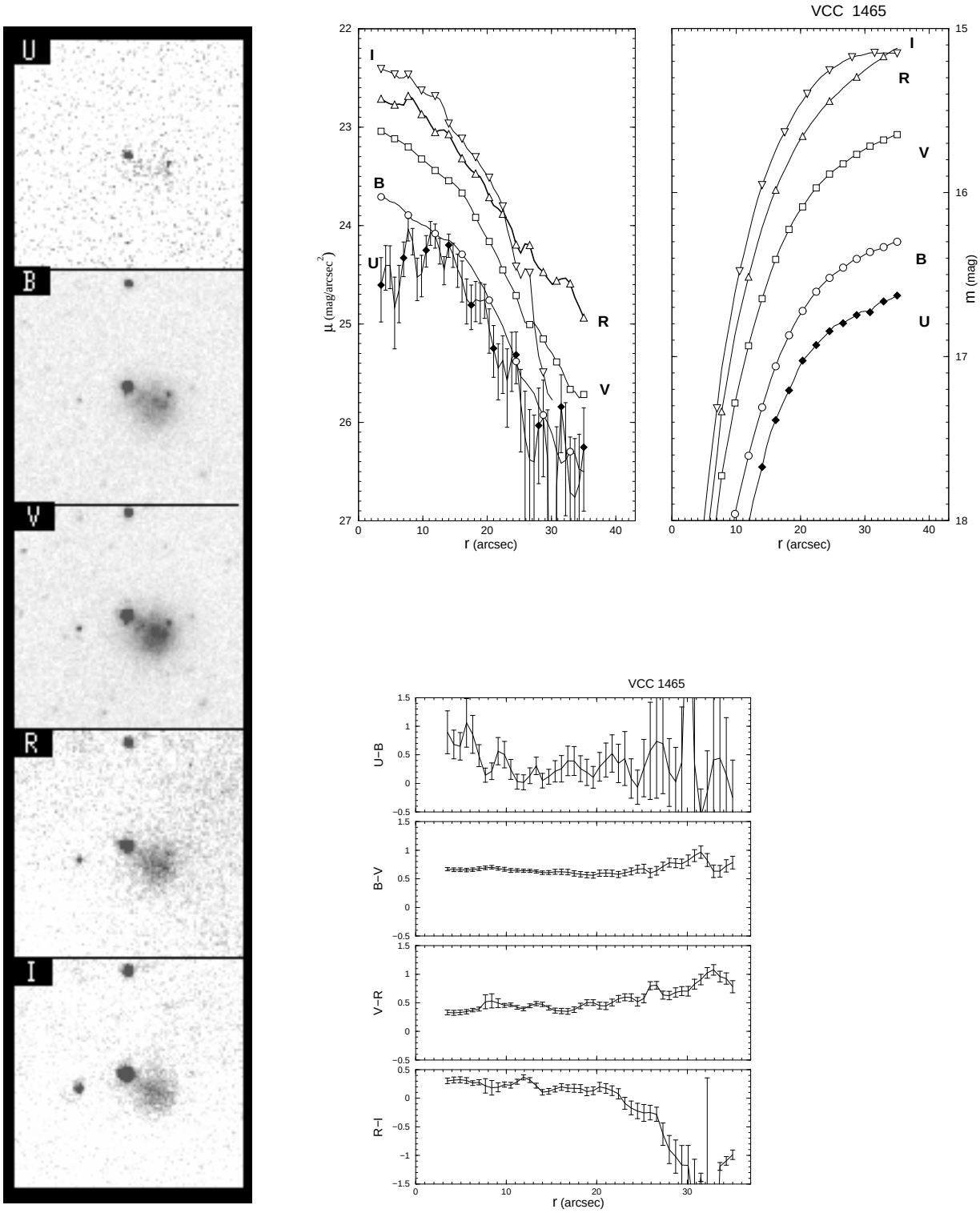

Fig. 21.— VCC 1465- Symbols as in Fig. 2

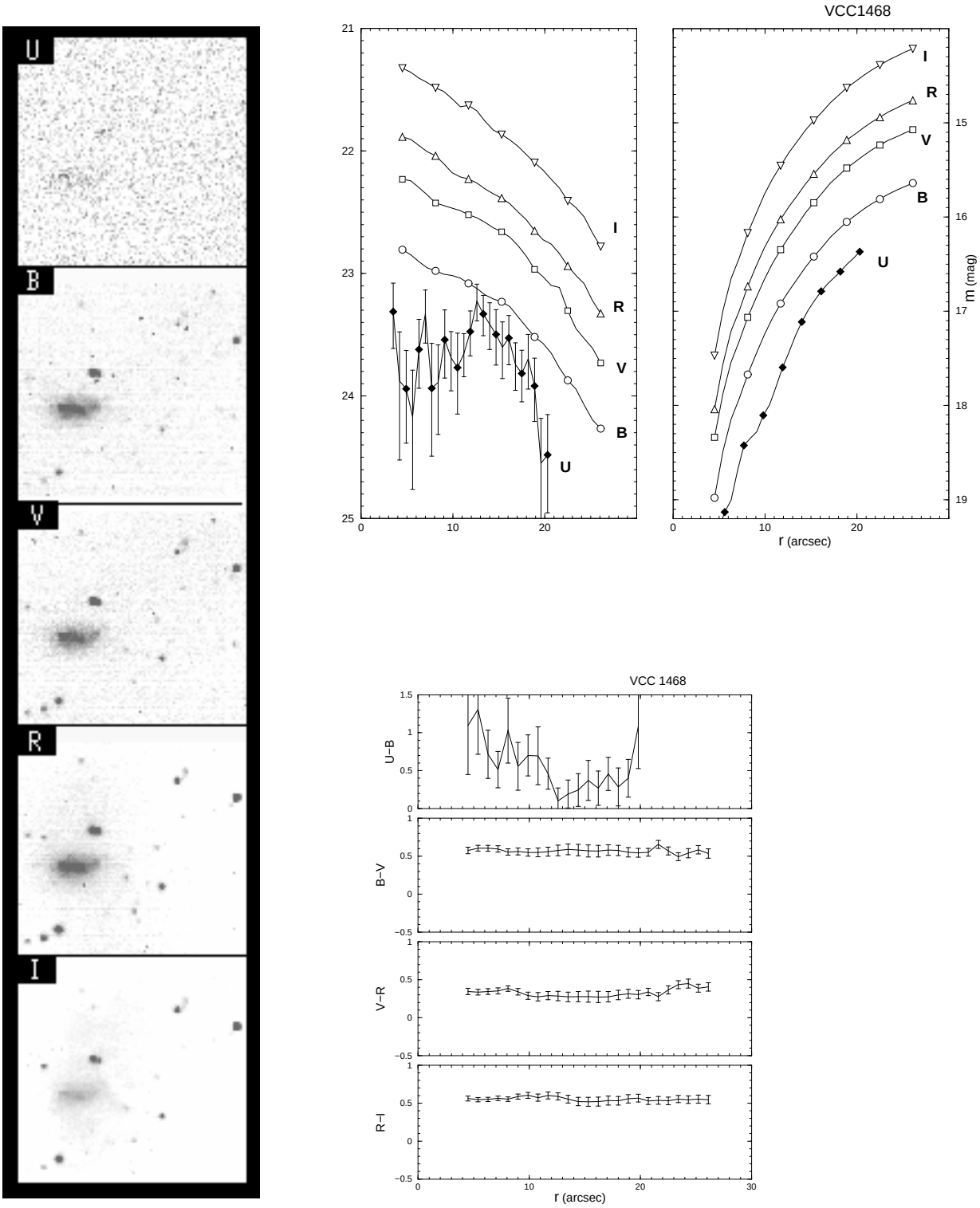

Fig. 22.— VCC 1468- Symbols as in Fig. 2

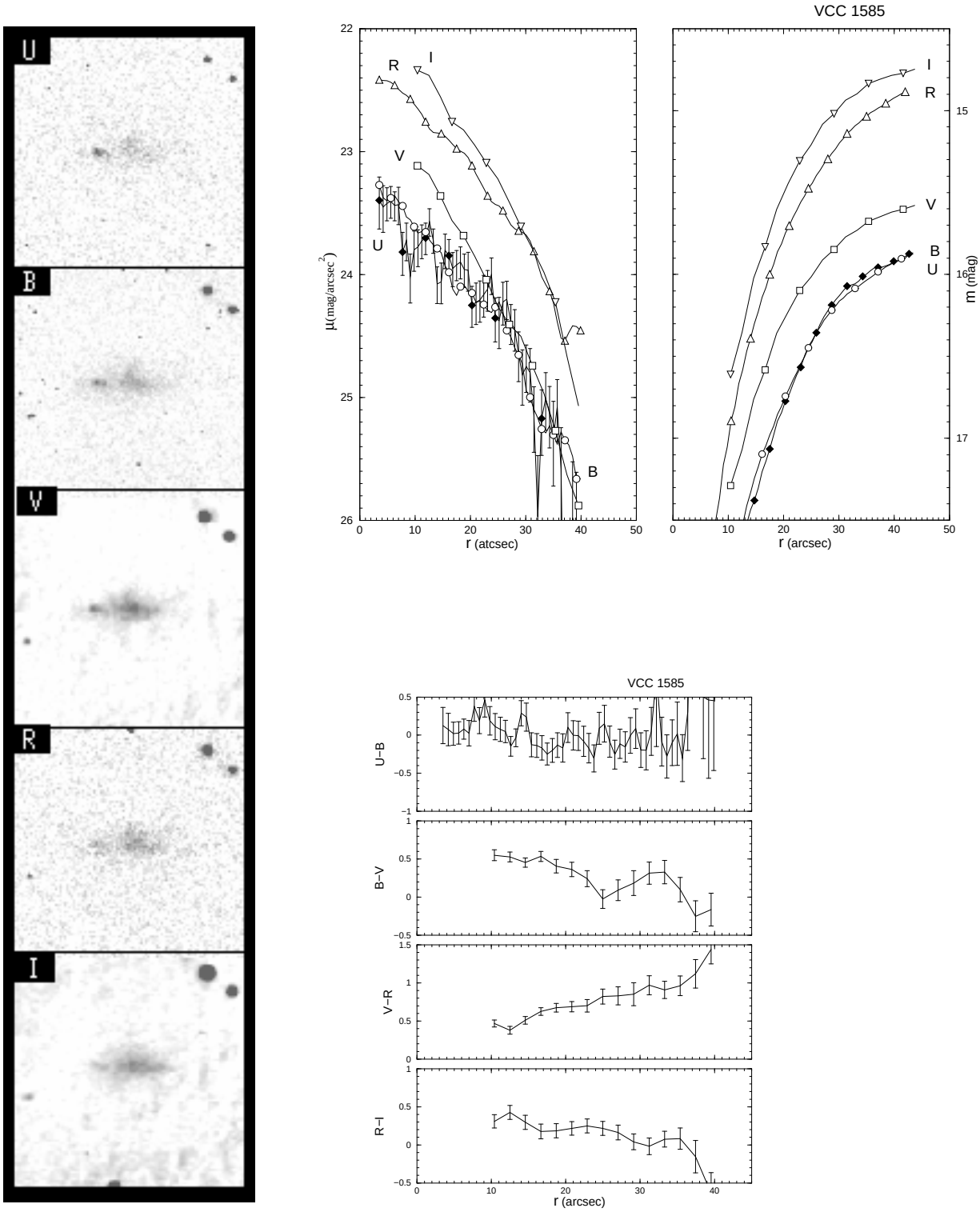

Fig. 23.— VCC 1585- Symbols as in Fig. 2

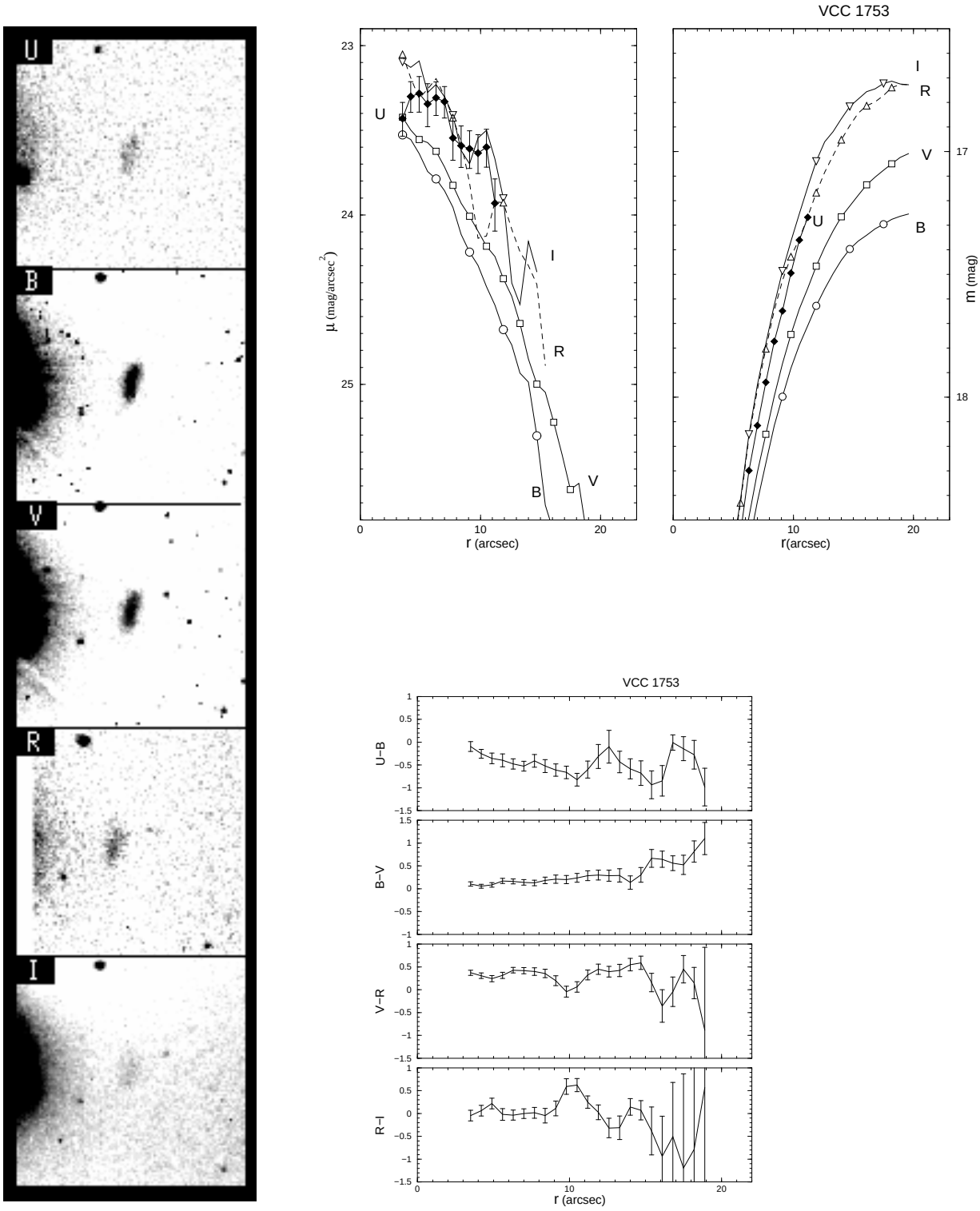

Fig. 24.— VCC 1753- Symbols as in Fig. 2

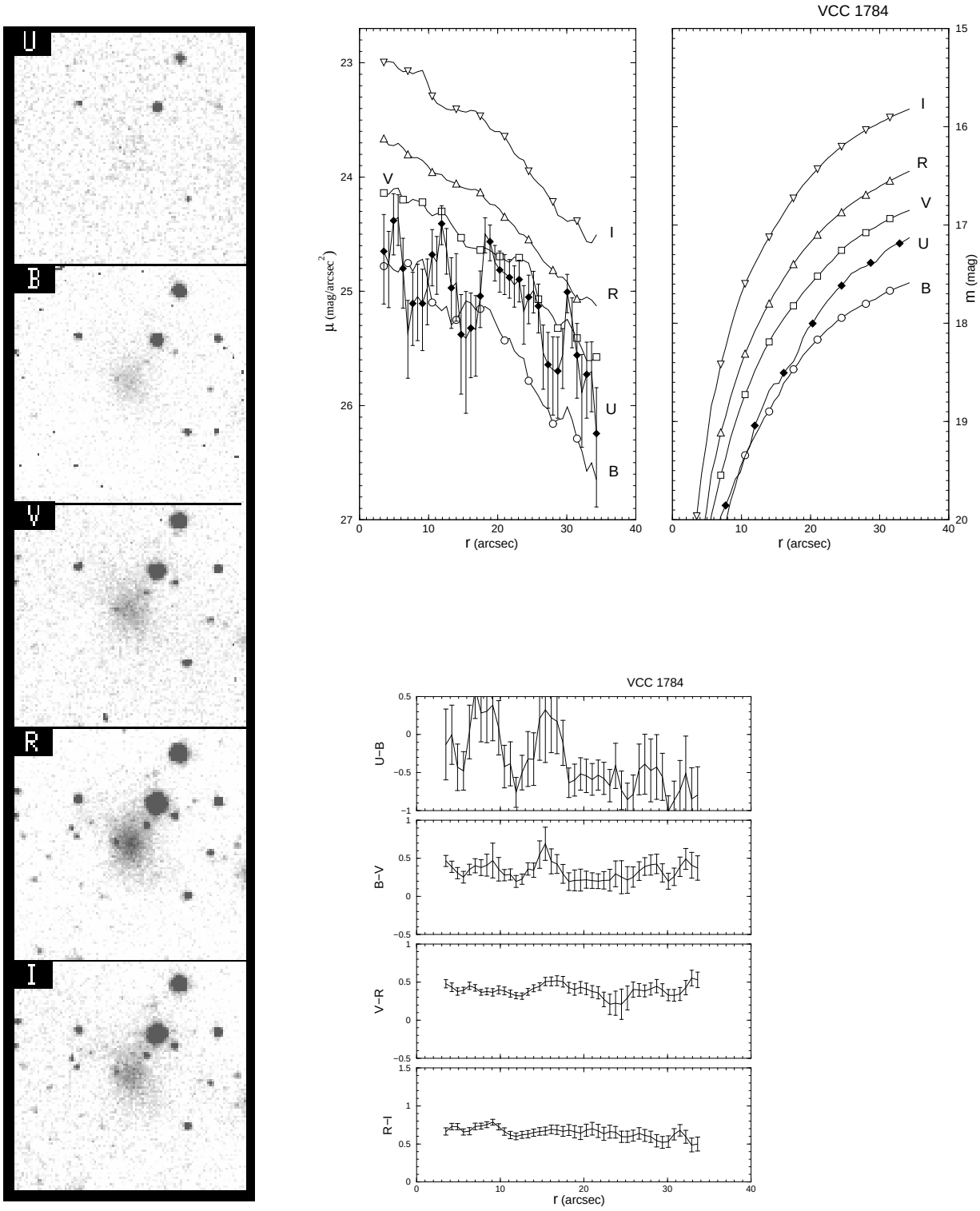

Fig. 25.— VCC 1784- Symbols as in Fig. 2

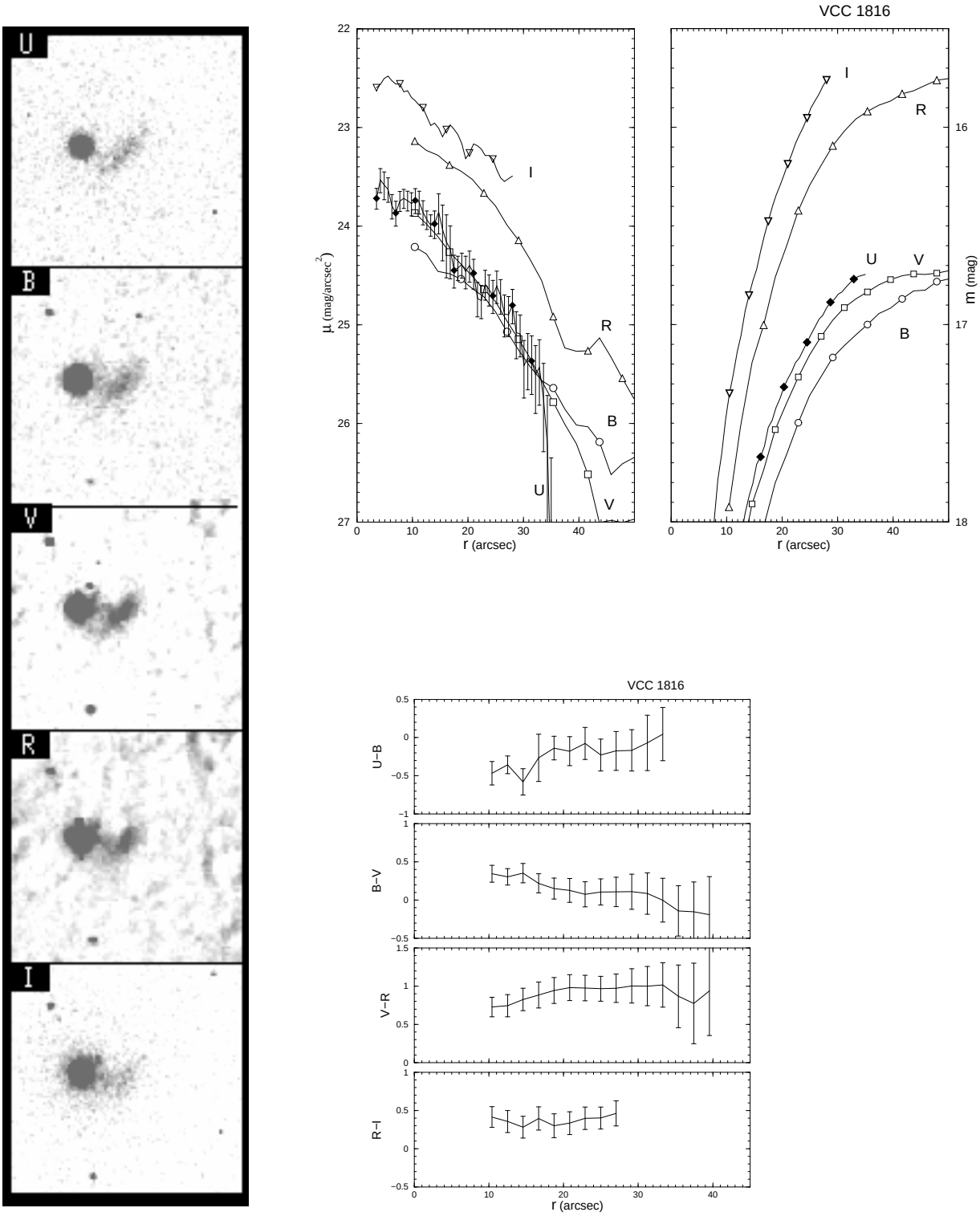

Fig. 26.— VCC 1816- Symbols as in Fig. 2

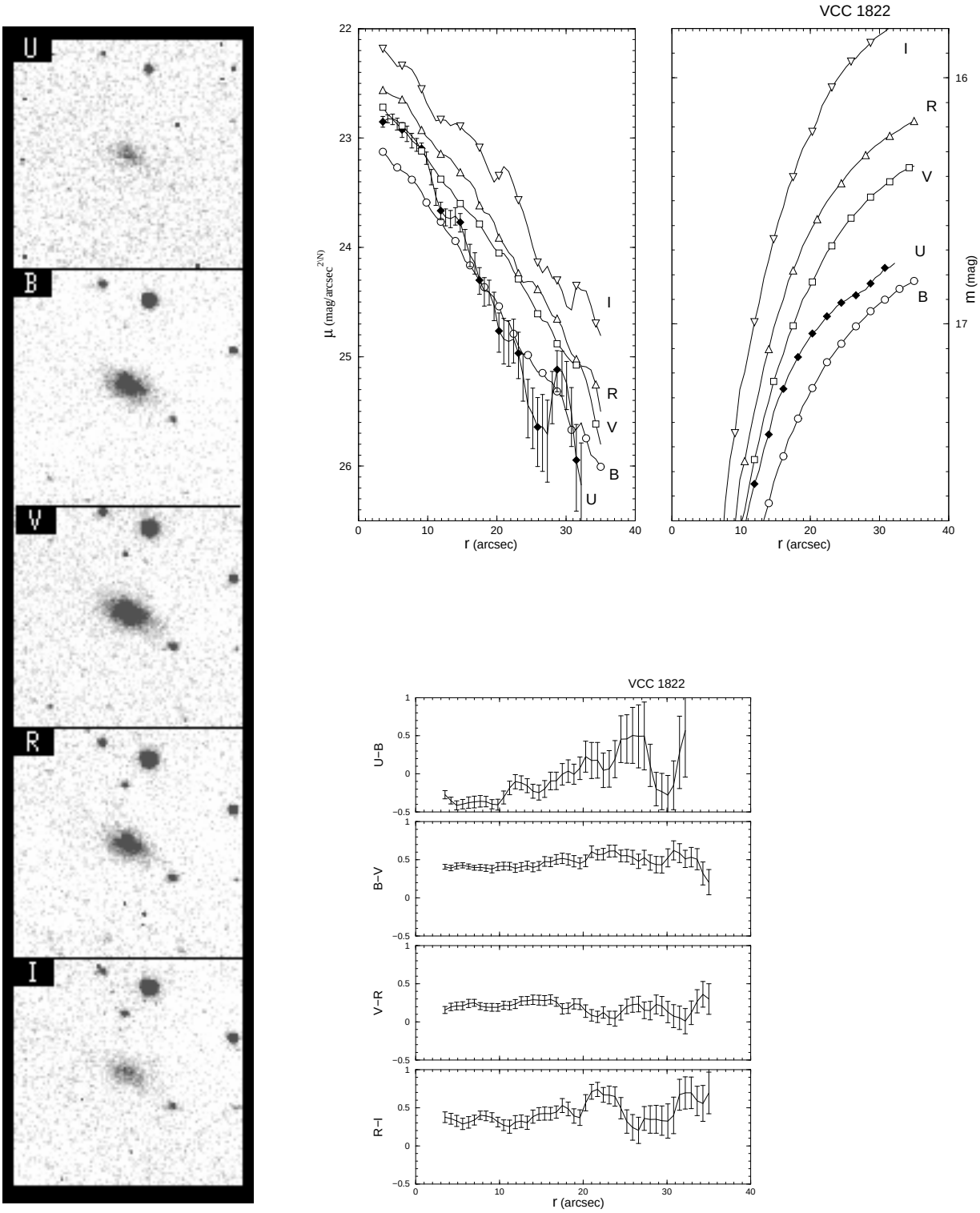

Fig. 27.— VCC 1822- Symbols as in Fig. 2

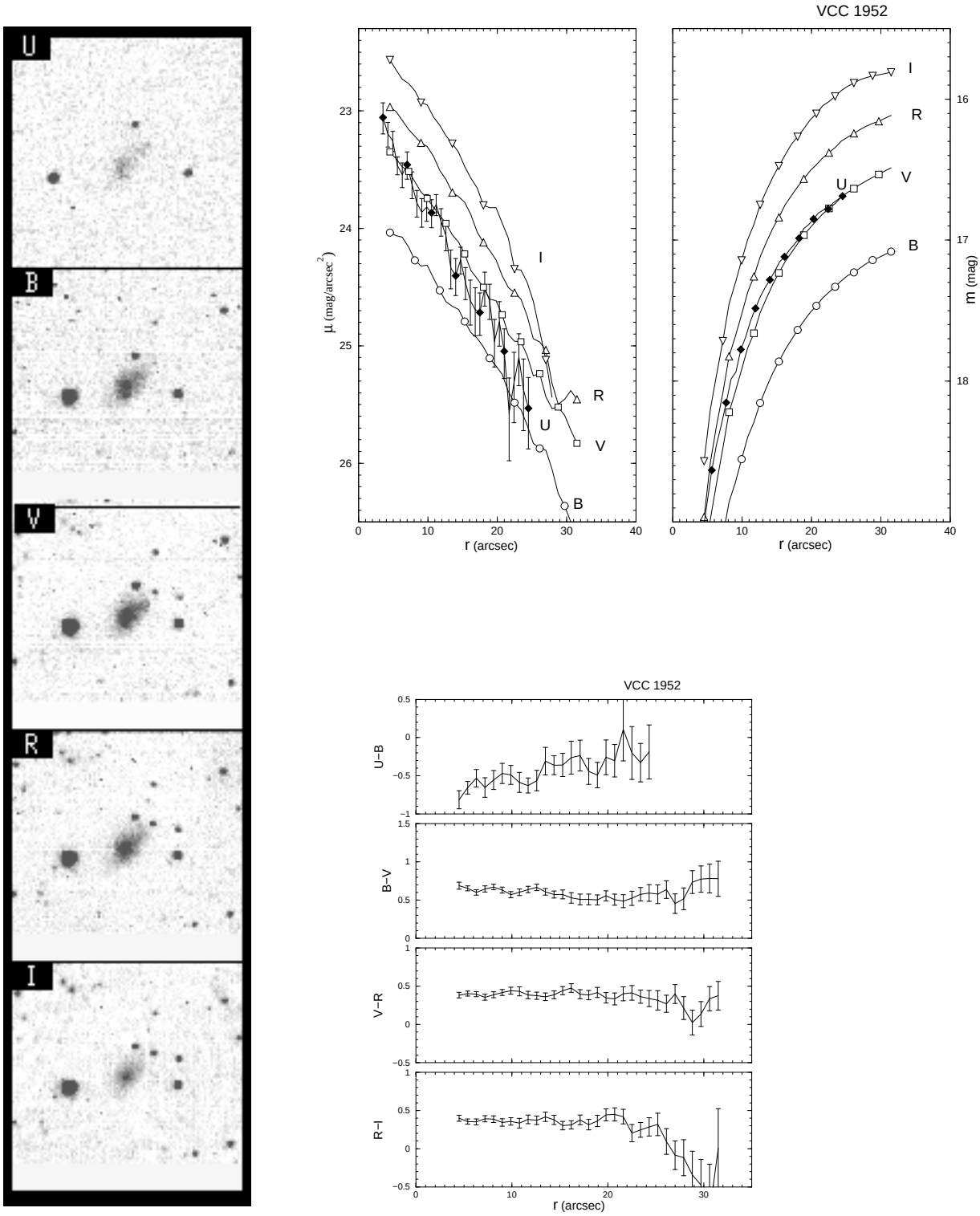

Fig. 28.— VCC 1952- Symbols as in Fig. 2

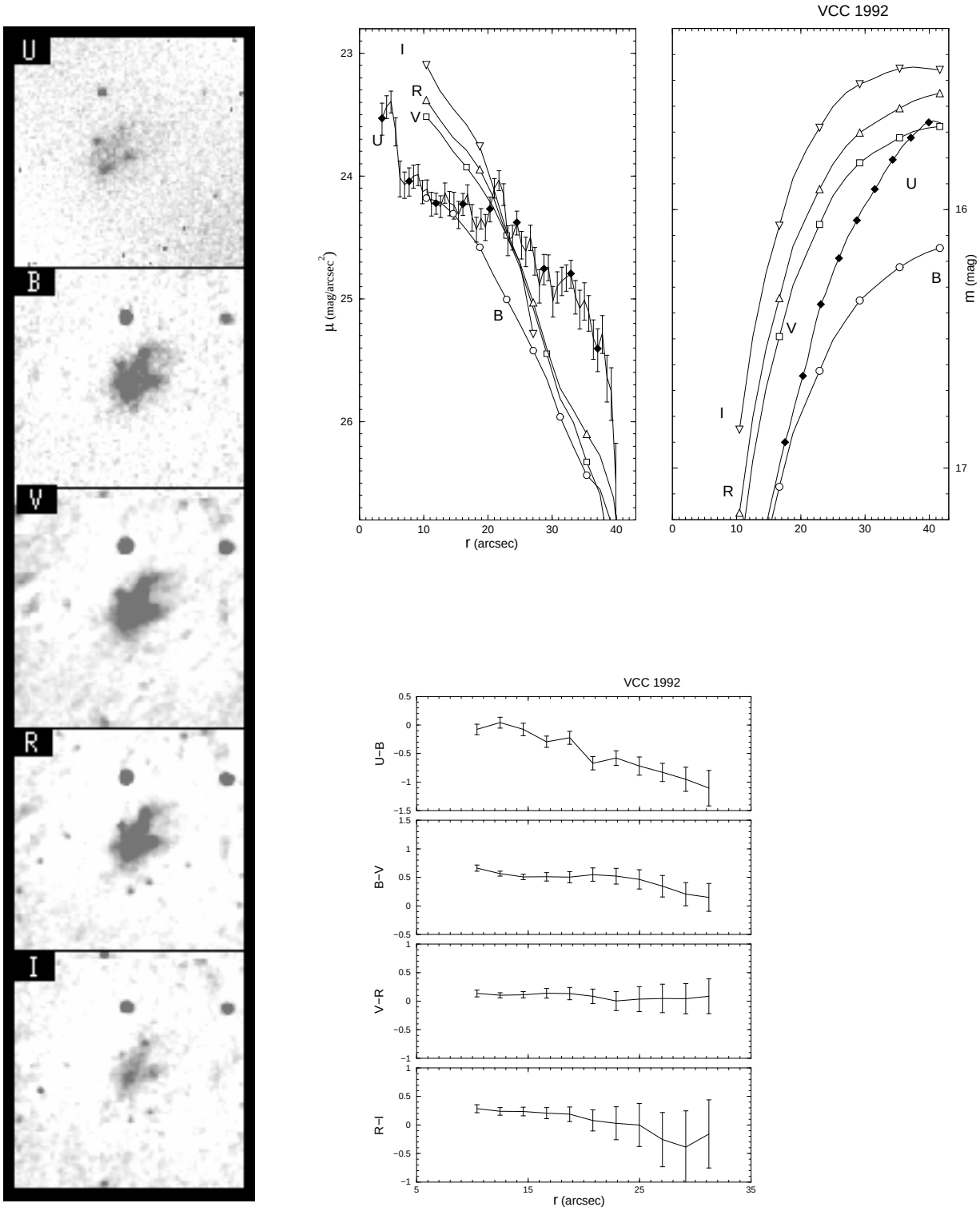

Fig. 29.— VCC 1992- Symbols as in Fig. 2

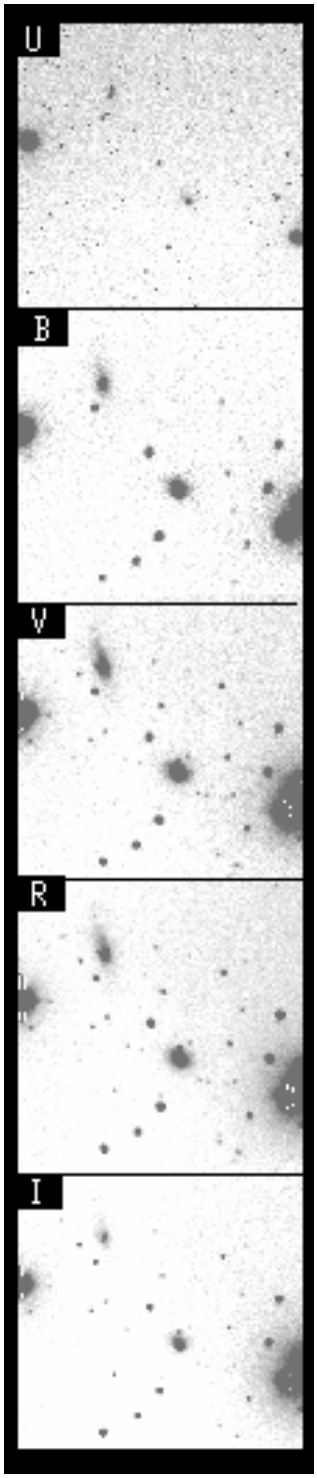

Fig. 30.— VCC 2037- No surface photometry. The galaxy is at the top-left part of the field. Note a superposed bright star covering most of the galaxy on all images. Also visible, at the center-right of the field, is VCC 2034, a blue compact galaxy (BCD)

Fig. 31.— Diagrams of color-color gradients per h_B.

Fig. 32.— Diagrams of color gradients (B-I) per h_B vs. lopsidedness index (A) of Hα emission. The data point with large error bars corresponds to VCC 169 discussed above.